Study of the Local Backprojection Algorithm for Image Formation in Ultra Wideband Synthetic Aperture Radar

Ishtiaque Ahmed

This thesis is presented as part of Degree of
Master of Science in Electrical Engineering

Blekinge Institute of Technology
December 2008

Blekinge Institute of Technology, Sweden
School of Engineering
Department of Electrical Engineering
Supervisor: Viet Thuy Vu, Thomas K. Sjögren
Examiner: Viet Thuy Vu

This thesis is submitted to the Department of Signal Processing, School of Engineering at Blekinge Institute of Technology in partial fulfillment of the requirements for the degree of Master of Science in Electrical Engineering with emphasis on Telecommunications. The thesis is equivalent to 20 weeks of full time studies.

Contact Information

Author:
Ishtiaque Ahmed
Email: isah06@student.bth.se, pavel_qmed@yahoo.com

University advisor(s):
Viet Thuy Vu
E-mail: viet.thuy.vu@bth.se
School of Engineering
Blekinge Institute of Technology, Ronneby.

Thomas K. Sjögren
E-mail: thomas.sjogren@bth.se
School of Engineering
Blekinge Institute of Technology, Ronneby.

Abstract

The purpose of this thesis project is to study and evaluate a UWB Synthetic Aperture Radar (SAR) data image formation algorithm, that was previously less familiar and, that has recently got much attention in this field. Certain properties of it made it acquire a status in radar signal processing branch. This is a fast time-domain algorithm named Local Backprojection (LBP).

The LBP algorithm has been implemented for SAR image formation. The algorithm has been simulated in MATLAB using standard values of pertinent parameters. Later, an evaluation of the LBP algorithm has been performed and all the comments, estimation and judgment have been done on the basis of the resulting images. The LBP has also been compared with the basic time-domain algorithm Global Backprojection (GBP) with respect to the SAR images.

The specialty of LBP algorithm is in its reduced computational load than in GBP. LBP is a two-stage algorithm — it forms the beam first for a particular subimage and, in a later stage, forms the image of that subimage area. The signal data collected from the target is processed and backprojected *locally* for every subimage individually. This is the reason of naming it Local backprojection. After the formation of all subimages, these are arranged and combined coherently to form the full SAR image.

Keywords: SAR, GBP, LBP, Image formation, Chirp, UWB, Time-domain, Subaperture, Subimage, Backprojection.

Acknowledgments

I would like to express my sincere gratitude to my supervisors Mr. Viet Thuy Vu and Mr. Thomas K. Sjögren for their continuous guidance and kind support throughout this thesis. Their considerate and friendly approach helped me be frank in discussing any problems with them. Their knowledgeable supervision, illustrative ways of explaining something helped me grasp some idea in an easy way. Without their expert guidance, it would not be possible to come to an end with this thesis.

I am ever grateful to Dr. Mats I. Pettersson for making me a way to work on a part of his project and for giving me the lab facilities in the Department of Signal Processing in Blekinge Institute of Technology, Ronneby.

I want to thank my friend Samiur Rahman who first informed me about this research group and its thesis opportunities and, helped me giving relevant literatures.

Finally, I want to express my hearty gratitude to my parents and family members for their immense support and encouragement that helped me much to complete this thesis.

Contents

List of Figures

List of Tables

Chapter 1

Introduction

1.1 Introduction

In the present day world, when technology is passing its golden era, so many revolutionary things have been invented for the welfare of mankind. Some inventions are directly related to the daily life of humans. Some are related in a way that is not so obvious. Electrical technology is a boon for the civilization, the testimony of which is very obvious. High-frequency communication engineering is a very strong and important sector of electrical engineering in the modern age. This thesis is about an application of ultra-wideband Synthetic Aperture Radars (SAR) operating in the VHF band (20 to 90 MHz).

This thesis is a study of an image formation algorithm, Local Backprojection (LBP) by name, that can be applied for very large aperture radars. The implementation of the algorithm is done in MATLAB based on the theories and mathematics described in [1] and [2]. Radar imaging is a common phenomenon in military activities and also used for civil purposes. The imaging could be of some item of interest be it on the ground or, in the air. Sometimes, solely the ground image is taken. Terrain imaging is done for diverse purposes like - tracing presence of minerals, investigating earth nature etc. Image of moving objects on ground or, flying objects are done in military and defense sector. In this study, a stationary point target on ground has been considered. Image formation of that point target has been performed using the algorithm and its performance has been evaluated also.

1.2 Thesis Paper Outline

A profile of this thesis paper is given here.

In **Chapter 2**, the fundamentals of radar technology starting from remote sens-

ing have been discussed. The backgrounds of SAR, its applications and, the essential geometry necessary for the imaging are covered. A brief of the SAR data processing algorithms are also given in this chapter.

Chapter 3 presents the important signal processing theories and, the interpolation methods necessary for this project.

Chapter 4 is all about the Global Backprojection algorithm. The images formed in this method have been shown. The effect of motion compensation is also discussed.

The main topic of this thesis, the Local Backprojection algorithm, is presented in **Chapter 5**. Image quality enhancement has also been a part of this chapter.

An assessment of the Local Backprojection algorithm has been performed in **Chapter 6**. The evaluation is done based on the resulting image quality for different parameter values.

Finally, in **Chapter 7**, the whole project has been summarized and some possible future works have been suggested.

Chapter 2

Fundamentals of Radar Engineering

2.1 Remote Sensing

Remote sensing, as it sounds, means to sense something from a place remotely located from that object. If the sensing or tracking is done from a place in contiguity of that particular object, it would no longer be called remote sensing. The purpose of remote sensing is to collect information on an area or an object from a distant location using specially designed devices.

The definition of remote sensing could be more specialized for the Radar technology as – "Remote sensing is the science (and to some extent, art) of acquiring information about the Earth's surface without actually being in contact with it. This is done by sensing and recording reflected or emitted energy and processing, analyzing, and applying that information."[3]

Airborne and spaceborne radars do continuously sense the earth surface from a long distance. These radars perform this sensing phenomenon using the electromagnetic (EM) waves in certain frequency bands.

2.2 Radar Technology

RADAR stands for RAdio Detection And Ranging. Radar technology is a good application of EM radiation. There is a big range of frequencies in EM spectrum. Radio waves are part of this spectrum holding certain band of frequencies.

Scottish scientist Robert Watson-Watt defined radar as follows - "Radar is the art of detecting by means of radio echoes the presence of objects, determining their direction and ranges, recognizing their character and employing data thus
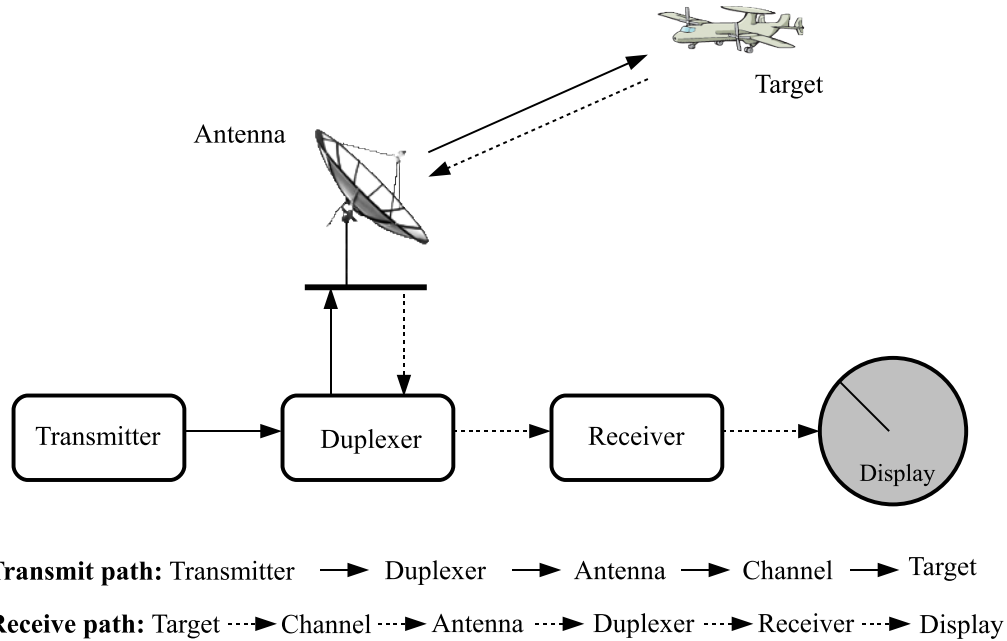
Figure 2.1: Basic radar system.

obtained in the performance of military, naval, or other operations."[4]

A radar system works exactly in the same principle as used in measuring distance by sound echoes, but here radio or microwave pulses are used instead of sound. There are one transmitter and one receiver in a radar system. The transmitter sends radio pulses and, the receiver picks up the reflected signals (echo) from a target on the ground or any other flying objects. Radars are sometimes classified according to the design of the system as regards the existence of the transmitter and receiver in it. Radars in which the transmitter and receiver are collocated, are called **'monostatic radars'**; and, those in which the transmitter and receiver are separated are called **'bistatic'**. A typical block diagram of a radar system could be as shown in Figure 2.1.

2.3   Synthetic Aperture Radar

Synthetic Aperture Radar (SAR) is basically used in remote sensing and satellite imaging. The true picture of SAR as a sensor is shown in Figure 2.2. In case of imaging, resolution of the imagery is of great concern and higher resolution in the azimuth direction is always desired. Resolution in the azimuth direction depends on beamwidth and distance to a target. Big antennas with short wave
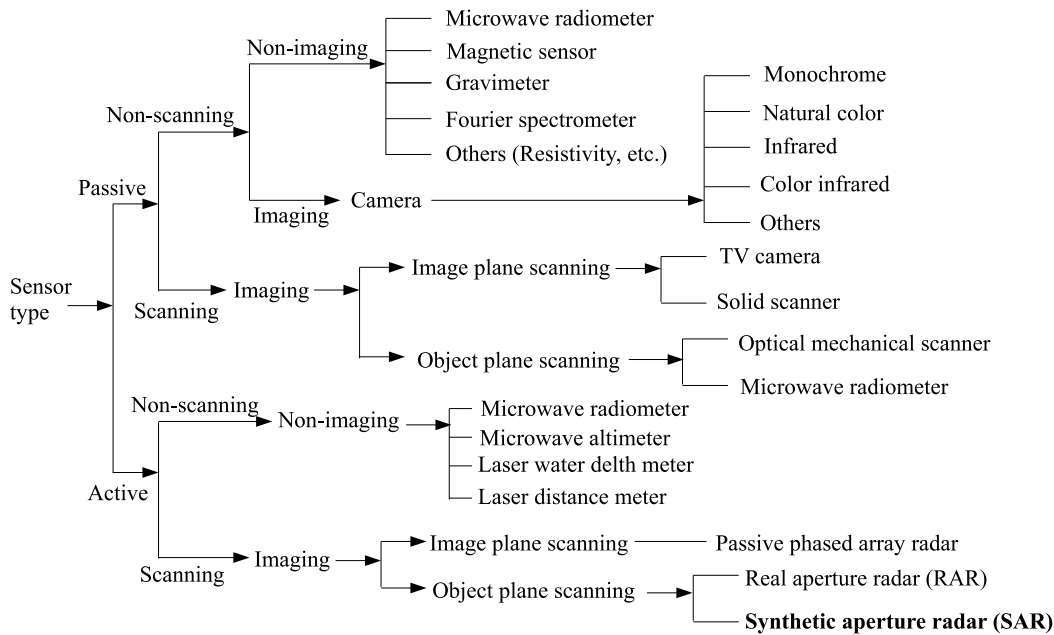
Figure 2.2: Sensor classification tree.

lengths of the transmitted signal can produce good resolution. Therefore, two things are important in this resolution matter: (i) antenna size and, (ii) wavelength. The wavelength can be varied easily by changing the frequency of the transmitted signal. Therefore, short wavelength can be achieved by using high frequency signals. However, the antenna size is an issue now. To increase the resolution in a Real Aperture Radar (RAR) system, the antenna has to be very big. Sometimes the antenna size might be required to be bigger than the aircraft itself mathematically with a view to having high resolution, which is impracticable in reality. This constraint made the way to think of something that could synthetically increase the aperture size (length).

Conventional RAR or SAR produces a very narrow effective beam, which gives the azimuth resolution of them before processing. Reduction of effective beamwidth will improve the azimuth resolution, and beamwidth is inversely proportional to the antenna aperture. Hence, large aperture will give narrow beamwidth and consequently improved resolution. Now, the question is: How can a large aperture be achieved? The formation of a synthetic aperture is considered as a collection of successive pulses transmitted and reflected in a sequence and the aperture is created in a computer. The aperture is synthesized as long as the target stays within the radar beam. Figure 2.3 shows the idea of aperture synthesis. Thus the SAR evolved from RAR. SARs have overcome the limitations of RARs.
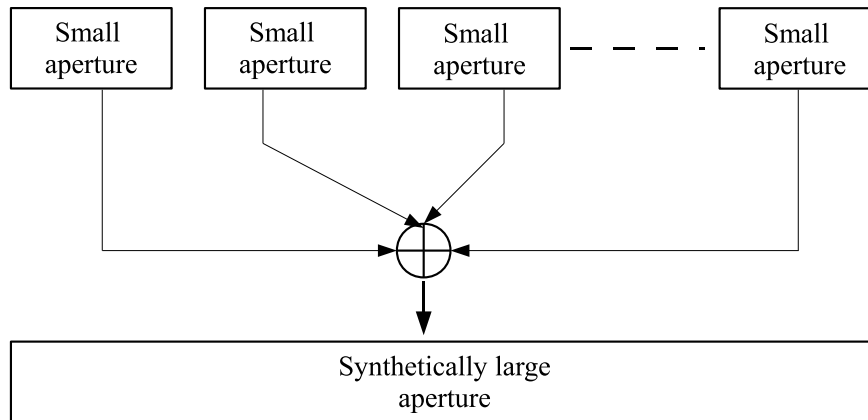
Figure 2.3: Concept of large aperture formation.

2.4   Applications of SAR

SARs are widely used as ground-imaging radars. The ability to mirror earth surface for displaying topography is a prime use of SAR for a variety of applications. Traditional infrared sensing technologies have been suppressed for a definite advantage of SAR over those. SARs have its own surface illuminating capability that allows it to work in hazy weather (fog, rain etc.) and even in night. During such unfavorable weather condition, the infrared remote sensing systems are inefficient.

SARs are of two types: (i) airborne and, (ii) spaceborne. Airborne systems are those operating on variety of aircrafts carrying equipment, while spaceborne systems operate on satellites or space shuttle platforms. The airborne systems provide regional coverage while the spaceborne systems provide global coverage on a periodic and an as-required basis as seen in Figure 2.4.

Some of the popular SAR systems are mentioned here, [2, 6]
     Airborne: *CARABAS-II, LORA, AIRSAR/TOPSAR, CCRS C/X SAR, DCS, IFSARE, P-3/SAR, STAR-1 & STAR-2.*
     Spaceborne: *ALMAZ-1, ERS-1, JERS-1, RADARSAT, SIR-C/X-SAR.*

Earth observation using SAR systems have wide range of applications [8]: The majority of applications of SAR systems are based on its imaging capability of the earth surface. Monitoring of Earth's continental ice sheets and marine ice cover, ocean wave measurement, frozen terrain studies, buried object detection and, other geological studies are mentionable applications of SAR systems that are conducted depending on the images a SAR produces. SAR imagery helps to trace the existence of minerals under the sea e.g. oil, gas etc. SAR systems can
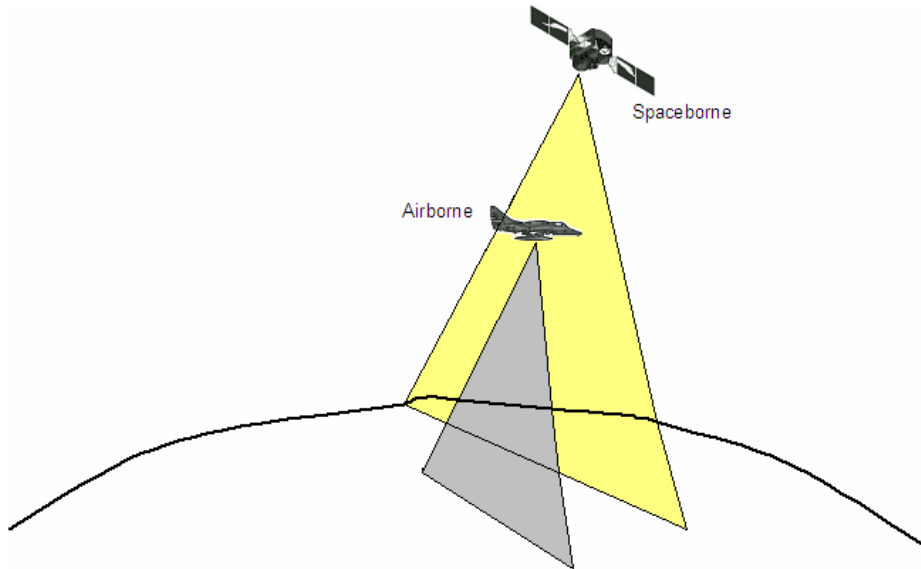
Figure 2.4: Classification of Radar.

detect the ships on oceans, their movement and motive. SAR GMTI [9] radar systems are particularly used for detecting, tracking and to have the additional functionality of imaging of moving targets on the ground in its surroundings [10–11].

UWB SAR systems have many applications both on the land and ocean. Low-frequency EM waves for its long wavelengths can penetrate into the foliage and also in some types of soil to some extent [7]. Such property of EM energy is utilized in FOPEN and GPEN radars. FOPEN radar systems are mostly used in military investigations, and for researches on geographical issues GPEN radar systems are involved. The property of cloud penetration makes SAR systems important in tropics areas. It helps in forestry and agriculture by mapping and monitoring the land. The functionality of SAR systems is independent of weather conditions and this makes it more priceless. SAR data can help estimate the damage on the land due to natural calamities and to optimize response initiatives.

2.5   Geo-coding Geometry

To understand the SAR operations and/or analyze or work with it, certain ge-
ometrical definitions have to be studied as a prerequisite. Some terminologies
related to synthetic aperture radar must be illustrated first.

The following picture is a very common one in the study of radar systems for
geographical imaging. We see a side-looking view in Figure 2.5.
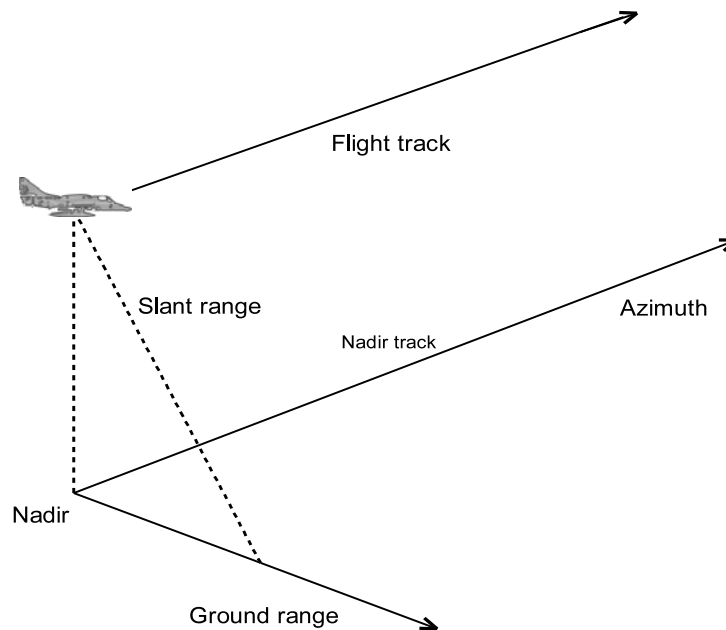
Figure 2.5: Sidelooking view of SAR scanning.

Azimuth indicates linear distance in the direction parallel to the radar flight
path. Azimuth is also known as along-track direction. The direction in 90° to
the azimuth direction is called **Ground range**. The point directly beneath the
radar is called **Nadir**, and the azimuth line is also sometimes termed as nadir-
track.

Figure 2.6 will give better understanding of the **Slant range**.

The state of scanning of a radar could be better understood from Figure 2.7.
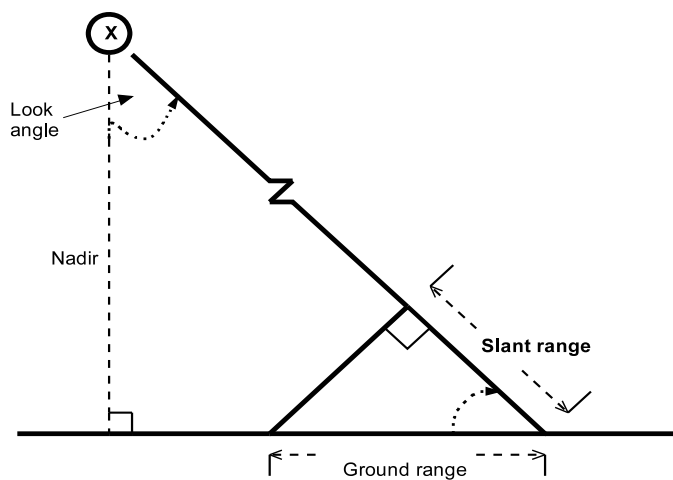
Figure 2.6: Slant range.

It shows a very typical picture of the radar and its relevant terms needed to study its functionality.
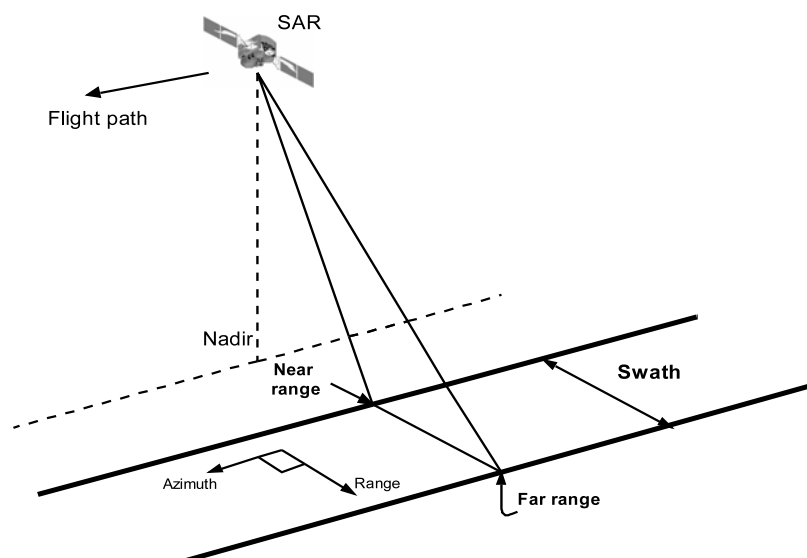
Figure 2.7: A picture of SAR scanning.

Swath is the piece of terrain where the radar focuses. The edge of the swath nearest to the nadir track is the **Near range** and the edge furthest is called the **Far range**.

There are some important angles in radar geometry. Those are: elevation angle, incidence angle, depression angle, aspect angle, integration angle and so on. In Figure 2.8 and 2.9 these angles are illustrated clearly.
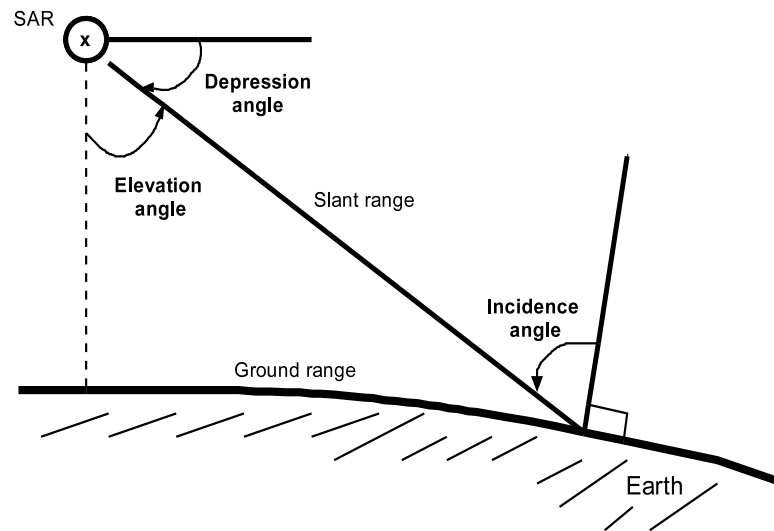
Figure 2.8: Geometric angles in radar engineering.
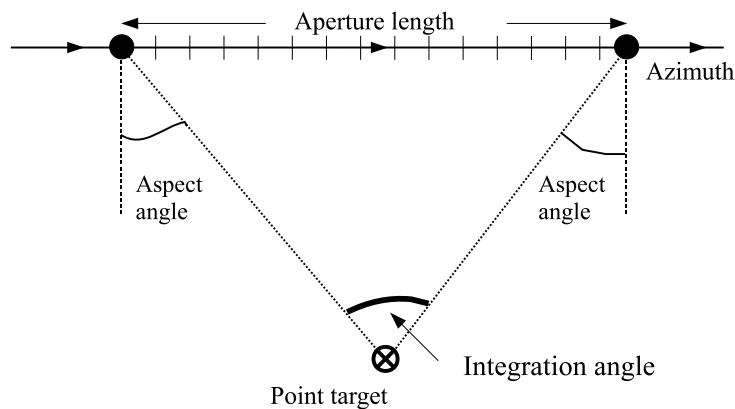
Figure 2.9: Integration angle.

Figure 2.10(a) depicts the signal transmission and collection phenomena as the SAR moves on along the $\overline{BA}$ direction. As a point target, a corner reflector is shown on the ground where from the signal is being reflected. A corner reflector is particularly chosen for its property of reflecting back the signal with minimum scattering. The received signal in a collective form is shown in Figure 2.10(b).
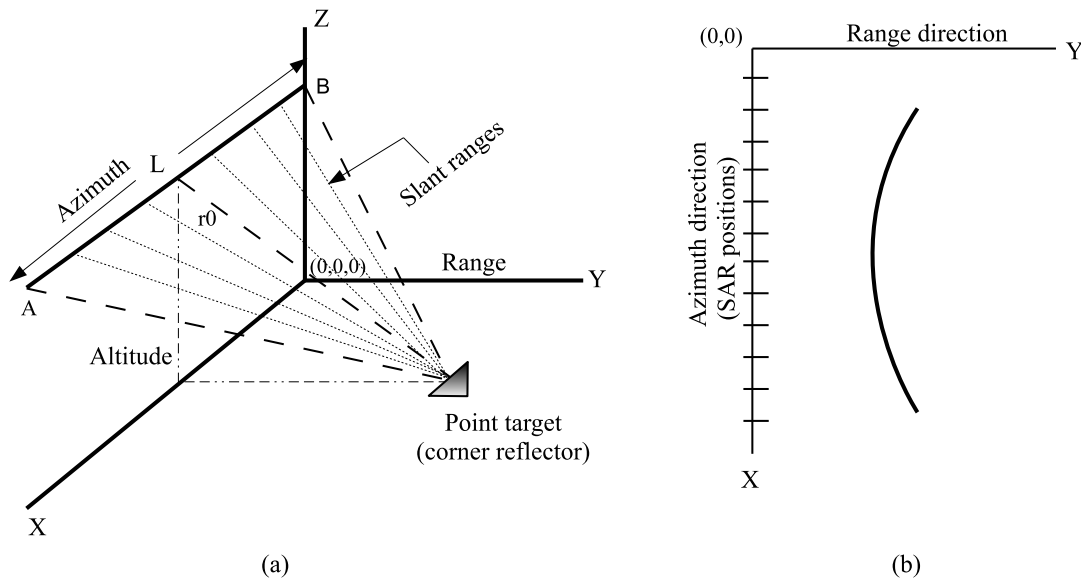
Figure 2.10: The (a) signal receiving scenario and, (b) signal history.

2.6   Imaging Algorithms

Image formation algorithms are classified in two classes: (i) FFT-based or, frequency domain methods, and (ii) time-domain methods. Time-domain methods are also called backprojection methods. There are several imaging algorithms in frequency and time domain. Algorithms in both domains have relative merits and drawbacks.

Some of the well-known frequency-domain algorithms are – Chirp Scaling (CS) algorithm [12], Range Migration (RM) algorithm [13], Polar Format (PF) algorithm, Range-Doppler (RD) algorithm [14]; while among the time-domain algorithms – Global Backprojection (GBP) [15], Fast Backprojection (FBP) [16], Local Backprojection (LBP) [1], and Fast Factorized Backprojection (FFBP) [17] are familiar.

2.6.1   Comparative Features of Imaging Algorithms

The frequency-domain methods are good in the issue of image processing since they try to reduce the processing load and they also produce good image quality for non-wideband (WB) SAR. However, for UWB SAR systems, they become unable to provide good quality imagery [2]. It is the long integration times, UWB SAR systems need, that makes frequency-domain methods inappropriate for good imaging. Long integration times require motion compensation for a good image. Therefore, time-domain backprojection algorithms work satisfactorily for UWB SAR systems, since they can provide adequate motion compensation to cope with the long integration times. However, frequency-domain algorithms can also provide motion compensation but, in fact, those are not very convenient to perform.

Most frequency-domain methods require interpolation of data in frequency domain. This causes another drawback of these methods. Due to data interpolation, sometimes different errors take place and these have some impact on the image produced resulting in degraded quality.

Frequency-domain algorithms have a major shortcoming depending on the nature of the aperture [17]. These algorithms go well for linear apertures, but not very suitable for the general non-linear aperture. Motion correction is again the main reason here, since motion compensation cannot be applied for the whole non-linear aperture at a time and, it is valid only locally if the total image is segmented in subimages. In time-domain algorithms, motion compensation is performed automatically for non-linear aperture and the image quality is the same as obtained for linear aperture.

Frequency-domain algorithms also need large computer memory to store and process big data. The dimension of data is related to the size of the image scene. For big scene size, the amount of data is going to be big and, thus it increases load on the processor. However, there is no scene size limitation in some time-domain algorithms (e.g. GBP). In another time-domain method (LBP), the data processing is done locally in segmented image area thus reducing the load on the computer memory [1].

Chapter 3

Signal Processing Fundamentals for SAR Processing

3.1 Introduction

In this chapter, the theoretical and mathematical preliminaries for radar signal processing issues have been covered and, these are described up to the depth as it was found necessary during the algorithm implementation. Chirp or, Linear FM signals are very commonly used in radar signal processing.

3.2 Chirp Signal

Chirp signals are also called Linear FM signals for its certain characteristics. The significance of the name Linear FM signals is lied on the frequency vs. time characteristic of the signal. The frequency of a chirp signal increases or decreases with time i.e., the instantaneous frequency is a *linear function of time*. Hence, the chirp signals are also termed technically as Linear FM signals. If a chirp signal is played in a speaker, it sounds like the chirping tone of birds and, this is the reason behind such naming. The chirp signal processing technique is also sometimes called CHIRP technique where CHIRP stands for Compressed High Intensity Radar Pulse.

The expression of the chirp signal that has been used as the transmitted signal in the implementation of this image formation algorithm is,

$$s(\tau) = A \operatorname{rect}\left(\frac{\tau}{T_p}\right) \exp\left\{j2\pi f_c \tau + j\pi K \tau^2\right\} \tag{3.1}$$

where, 'rect' implies a rectangular function of time τ and pulse duration T_p. f_c is the center frequency of the frequency band that have been used and, K is called the chirp rate (Hz/s) that is, the ratio of bandwidth B to the pulse duration i.e.

$K = (\frac{B}{T_p})$. The plot of the transmitted chirp signal is shown in Figure 3.1. Also the spectrum of the transmitted chirp is shown in Figure 3.2.
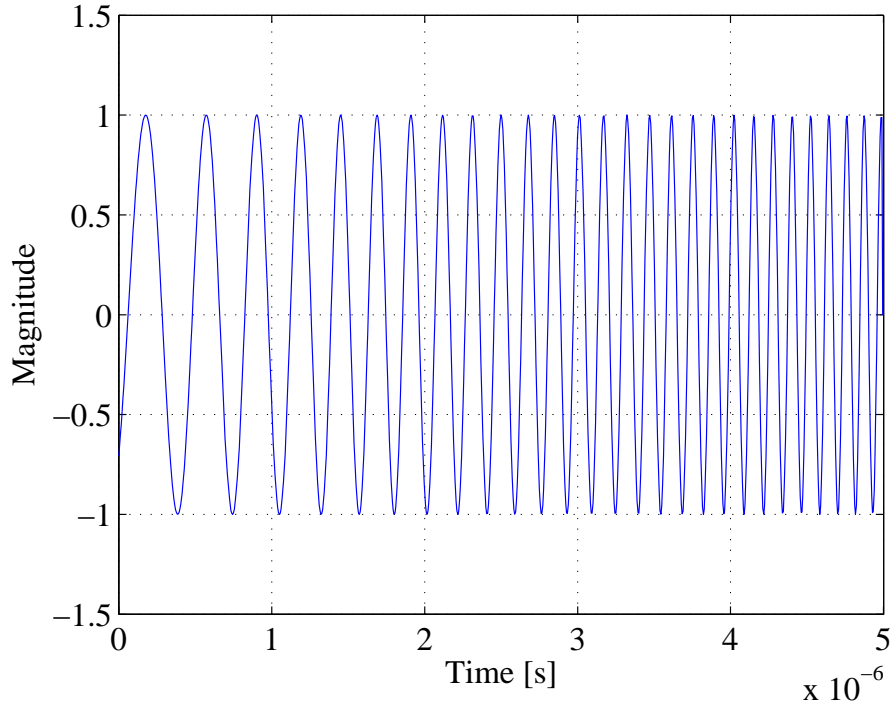
Figure 3.1: Transmitted chirp signal.

3.3   Pulse Compression

Image quality is a very important issue in the SAR image formation processes. The resolution of the SAR image of the target that is sensed must be very high in order for the image to be of nice quality. Parameters such as distance, speed etc. of a remote object are usually measured by strong pulse signals. In order to differentiate between two point targets, short-duration pulses must be used. In the image formation process in SAR systems, the signals reflected from the target are compressed for some definite purposes like, to maximize SNR, to achieve good image quality of the target and so. This received pulse compression is performed by matched filtering where linear FM pulse signal is convenient to deal with.

For UWB SAR systems, the pulse duration is inversely proportional to the PRF, therefore, short duration pulse can be obtained by using high PRF value.

$$T_p = \frac{1}{PRF} \tag{3.2}$$
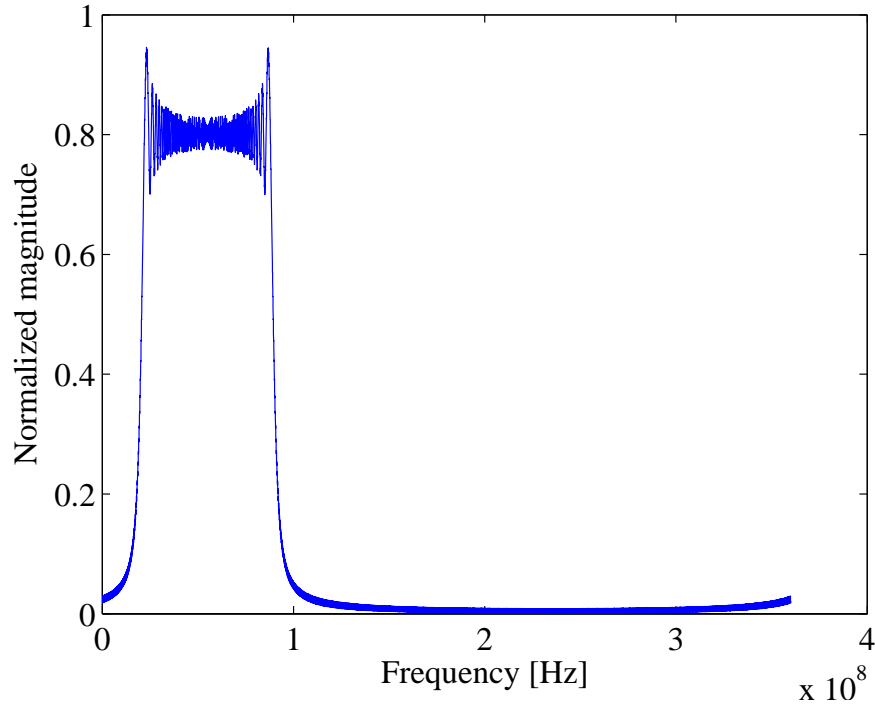
Figure 3.2: Spectrum of the transmitted chirp signal.

There is a minimum threshold in the selection of the PRF value. Half of the PRF value must be greater than or equal to the Doppler frequency, f_D as shown in (3.3).

$$\frac{PRF}{2} \geqslant f_D \tag{3.3}$$

The Doppler frequency equation is,

$$f_D = \frac{2V_{ave}}{c} \cdot f_{max} \cdot \sin\left(\frac{\theta_0}{2}\right) \tag{3.4}$$

where, V_{ave} is the average platform velocity, f_{max} is the upper frequency limit of the band, θ_0 is the integration angle and, c is the speed of light.

The pulse compression can be done by the 'matched filtering' technique. The pulse compressed form of the chirp signal in Figure 3.1 is shown in Figure 3.3.

3.3.1 Matched Filtering

In the context of matched filtering, convolution is a very important mathematical operation. Linear convolution can be used to apply matched filtering in time domain. In some books, 'matched filter' has also been termed as 'convolution
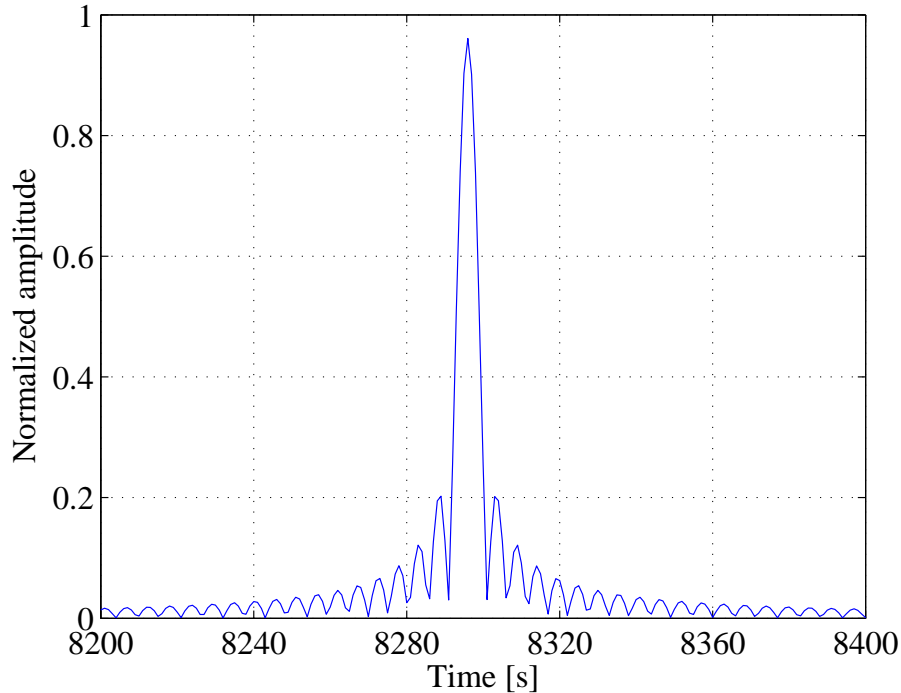
Figure 3.3: Received signal after pulse compression.

filter', since the output of the matched filtering is obtained from this convolution operation [18]. There is an explanation of such naming of a filtering method. Let us suppose, we have signal $s(\tau)$ with certain properties and, we want this signal in a different form, e.g. in a compressed form, $s_{mf}(\tau)$. A matched filter $h(\tau)$ can help in this matter. The filter is matched to the desired phase of the signal $s(\tau)$. The expression of a matched filter depends on the signal expression of $s(\tau)$. The matched filter is the time-reversed complex conjugate of the signal to be modified. Now, if the signal $s(\tau)$ is convolved with the matched filter $h(\tau)$ containing the desired signal properties (phase), it comes out in its desired form $s_{mf}(\tau)$. The phase match is the key subject here. Hence, it is called matched filtering.

3.3.2   Derivation of the Matched Filter Output

The convolution operation is forcing the signal $s(\tau)$ to be influenced by the signal properties of the matched filter $h(\tau)$ in order to bring out the desired form of the signal. This is somewhat like filling a casing with melted glass to give it the shape. If we consider the whole operation as convolution, then the casing is the matched filter and the melted glass is the signal $s(\tau)$.

The derivation of the matched filter output $s_{mf}(\tau)$ is shown here in convolution integral [18]. The convolution integral can be written as,

$$
\begin{aligned}
s_{mf}(\tau) &= s(\tau) * h(\tau) \\
&= \int_{-\infty}^{+\infty} s(u)h(\tau - u) \ du
\end{aligned}
\tag{3.5}
$$

We need to compress the received signal in this work. If the time domain complex linear FM signal given by (3.1) is the transmitted signal and, if the echo is received after a certain time delay (the time delay has been ignored for brevity), the received signal can be expressed as the following with f_c set to zero,

$$
s_r(\tau) = \text{rect}\left(\frac{\tau}{T_p}\right)\exp\{+j\pi K\tau^2\}
\tag{3.6}
$$

The matched filter $h(t)$ is then,

$$
h(\tau) = \text{rect}\left(\frac{\tau}{T_p}\right)\exp\{-j\pi K\tau^2\}
\tag{3.7}
$$

From (3.5) we get the matched filter output

$$
\begin{aligned}
s_{mf}(\tau) &= s_r(\tau) * h(\tau) \\
&= \int_{-\infty}^{+\infty} \text{rect}\left(\frac{u}{T_p}\right)\text{rect}\left(\frac{\tau-u}{T_p}\right)\exp\{j\pi Ku^2\}\exp\{-j\pi K(\tau-u)^2\} \ du \\
&= \int_{-\infty}^{+\infty} \text{rect}\left(\frac{u}{T_p}\right)\text{rect}\left(\frac{\tau-u}{T_p}\right)\exp\{j\pi Ku^2\}\exp\{-j\pi K\tau^2 + j2\pi K\tau u - j\pi Ku^2\} \ du \\
&= \exp\{-j\pi K\tau^2\}\int_{-\infty}^{+\infty} \text{rect}\left(\frac{u}{T_p}\right)\text{rect}\left(\frac{\tau-u}{T_p}\right)\exp\{j2\pi K\tau u\} \ du
\end{aligned}
\tag{3.8}
$$

To evaluate the integral, (3.8) has to be divided into two parts: one part where the signal is to the left of the matched filter, and the other part where it is to the right. Changing the integration limits, the integral in (3.8) becomes

$$
\begin{aligned}
s_{mf}(\tau) = \exp(-j\pi K\tau^2)\Bigg[&\text{rect}\left(\frac{\tau+\frac{T_p}{2}}{T_p}\right)\int_{-\frac{T_p}{2}}^{\tau+\frac{T_p}{2}} \exp(j2\pi K\tau u) \ du \\
&+ \text{rect}\left(\frac{\tau-\frac{T_p}{2}}{T_p}\right)\int_{\tau-\frac{T_p}{2}}^{\frac{T_p}{2}} \exp(j2\pi K\tau u) \ du\Bigg]
\end{aligned}
\tag{3.9}
$$

Simplification of (3.9) gives us the matched filter output

$$
\begin{aligned}
s_{mf}(\tau) \\
= (\tau + T_p) \, \mathrm{rect}\!\left(\frac{\tau + \frac{T_p}{2}}{T_p}\right) \mathrm{sinc}[K\tau(\tau + T_p)] + (T_p - \tau) \, \mathrm{rect}\!\left(\frac{\tau - \frac{T_p}{2}}{T_p}\right) \mathrm{sinc}[K\tau(T_p - \tau)] \\
= (T_p - |\tau|) \, \mathrm{rect}\!\left(\frac{\tau}{2T_p}\right) \mathrm{sinc}[K\tau(T_p - |\tau|)]
\end{aligned}
\tag{3.10}
$$

For certain TBP (Time Bandwidth Product) values, the expression of the compressed output can be approximated simply by

$$
s_{mf}(\tau) \approx T_p \, \mathrm{sinc}(KT_p\tau)
\tag{3.11}
$$

3.4   Interpolation

SAR images are comprised of complex data points or pixels. Points with different signal strength are represented with different colors in MATLAB. The maximum information are fetched from the points with strong received pulses. The raw SAR image contains much noise in it. Interpolation methods have been applied in order to remove those noise to some extent from the image and get a nicer one. The signal data was upsampled beforehand the application of the interpolation methods. Combination of upsampling of the data followed by interpolation operation gave more exact image scene. Several interpolation methods have been tested in this image quality improvement task; those are:

- Linear interpolation method

- Nearest-neighbor interpolation method

- Sinc interpolation method

An assessment of these methods had also been done by checking the time duration needed to produce the image after interpolation in each method.

3.4.1   Linear interpolation

In mathematics, interpolation is the problem to find or estimate the value of some point with respect to the values of some surrounding known points. Linear interpolation is the most commonly used interpolation method. In this method, the points to find out lie between the two certain known points, and these are existed on a straight line. Hence the name of this method is *linear* interpolation. There are two variables in this method; one is depended on the other.

Let us suppose, we have two known points (x_1, y_1) and (x_2, y_2). We need to know some intermediate value (x, y) between these two points. Here, y is the dependent variable and x is the independent. Values of y are obtained depending on the corresponding values of x. As mentioned earlier, all intermediate points will stay on a straight line and hence in order to find the value of y for a certain value of x, the following equation can be adopted from geometry,

$$\frac{y - y_1}{y_2 - y_1} = \frac{x - x_1}{x_2 - x_1} \tag{3.12}$$

Equation (3.10) gives the value of y as follows,

$$y = y_1 + (x - x_1)\frac{y_2 - y_1}{x_2 - x_1} \tag{3.13}$$

or,

$$y = y_1 + (x - x_1) \cdot m \tag{3.14}$$

Here, m represents the *slope* of the straight line,

$$m = \frac{y_2 - y_1}{x_2 - x_1} \tag{3.15}$$

Thus the coordinate position of an intermediate point can be found by linear interpolation. In SAR image formation, this interpolation method works very satisfactorily in noise elimination and improving the image quality.

3.4.2   Nearest-neighbor interpolation

The nearest-neighbor interpolation is perhaps the simplest form of interpolation method. The principle of this method is explicit from its name **'nearest-neighbor'**. This algorithm considers the value of the nearest point i.e., the point with maximum proximity. That is why this algorithm is also sometimes called *proximal interpolation*. Nearest-neighbor method is used widely in image processing due to its advantage of fast speed in operation. Implementation of this interpolation algorithm is easier than any other methods. It works well with over-sampling.

3.4.3   Sinc interpolation

For bandlimited signals, Sinc interpolation is a perfect interpolation method. In this method, the interpolation kernel is based on a sinc function. Shannon's sampling theorem conditions have to be satisfied to implement this algorithm. The conditions are [18]:

- the highest frequency of the signal to be sampled has to be finite i.e. the signal must be bandlimited.

- the sampling must avoid aliasing by following the Nyquist criterion. To retrieve the original signal avoiding aliasing, the sampling rate (f_s) must be greater than twice the baseband bandwidth (Nyquist rate, $2B$) or, in other words, the Nyquist frequency $(f_s/2)$ has to be higher than the baseband bandwidth (B). The following two expressions describe the Nyquist criterion well:

$$f_s > 2B \tag{3.16}$$

The interpolation kernel is a sinc function expresses as

$$h(t) = \text{sinc}(t) = \frac{\sin(\pi t)}{\pi t} \tag{3.17}$$

And, the interpolation is the summation of convolutions between certain number of samples of the signal $Y(i)$ and the sinc function. The interpolation can be mathematically expressed as

$$y(t) = \sum_i Y(i) h(t - i) \tag{3.18}$$

Implementation of this interpolation algorithm requires a bit deeper mathematical concepts, however, Sinc interpolation serves with very good performance in image quality enhancement.

Chapter 4

Global Backprojection

4.1 Introduction

The Global Backprojection (GBP) algorithm is the root of all time-domain algorithms for UWB SAR in image scene construction. GBP is the first time-domain algorithm which has been introduced with several advantages. Other backprojection algorithms are developed on it. Evaluation of any new time-domain algorithm is performed by a comparison of the proposed algorithm with GBP. Being a basic algorithm for SAR image formation, GBP possesses several advantages and disadvantages. The computational load (i.e. number of operations) in GBP is higher than other successor algorithms, and this load increases proportionally with the size of the image. For an image space of $N_x \times N_r$ pixels and N_a aperture positions, the number of operations GBP needs is proportional to $N_a \times N_x \times N_r$; where, N_x is the number of image pixels in the azimuth and, N_r is the number of image pixels in the range direction. However, despite such computational drawback, GBP provides some unique features. UWB low-frequency SAR systems require extreme range migration and motion compensation that GBP can provide. Moreover, there is no limitation of scene size focused by the SAR in this algorithm.

4.2 Image Processing and Formation

As mentioned in Section 2.3, the formation of a synthetic aperture is considered as a collection of successive pulses transmitted and received in a sequence and the aperture is created in a computer. The signal data acquisition phenomenon is mentioned here once again: at first, consecutive chirp signals are transmitted from the transmitter antenna in the SAR system. The signals are reflected back to the receiver antenna successively. Now the received pulses are compressed (Section 3.3) to have a good resolution of the SAR image. The compressed pulses are collected in a suitable way for processing.

In the study of GBP algorithm, the important SAR parameters and their values that have been considered during the simulation are tabulated in Table 4.1. The same parameter values are applicable to LBP algorithm (Chapter 5) also unless otherwise mentioned.

Table 4.1: SAR parameters.

Parameter	Value
Frequency band (VHF)	20 - 90 MHz
Altitude	2000 m
Ground range	1500 m
Integration angle	$45\,^\circ$
Platform velocity	128 m/s
Pulse repetition frequency (PRF)	100 Hz
Full aperture length	2071 m
Number of aperture positions	1618

4.2.1   Data Acquisition

In the algorithm implementation stage, all the received signals had been compressed and then they were arranged in a matrix form to make it suitable for the data processing part. Matched filtering (as mentioned in Section 3.3.1) had to be performed for the pulse compression. The matched filter is the time-reversed and complex conjugate form of the transmitted signal (3.1),

$$
s_r(\tau) = \text{conj} \left\{ \text{rect} \left(\frac{\tau_t}{Tp} \right) \exp \left[j2\pi f_c \left(-\tau_t + \frac{Tp}{2} \right) + j\pi K \left(-\tau_t + \frac{Tp}{2} \right)^2 \right] \right\}
\tag{4.1}
$$

Then, all the reflected compressed pulses are collected together and the collective view of the reflected signal data is a bow-shaped curved line (Figure 4.1), from which the received signal strength with reference to the point target at different aperture positions are realized.

The received signal quantity here is not a single signal rather a number of signals which is equal to the total number of aperture positions considered since, radio waves are transmitted from and received at every aperture point along the flight track of the SAR. For the matched filtering purpose, convolution operation is a must and for discrete signals, like the case here (we have number of received
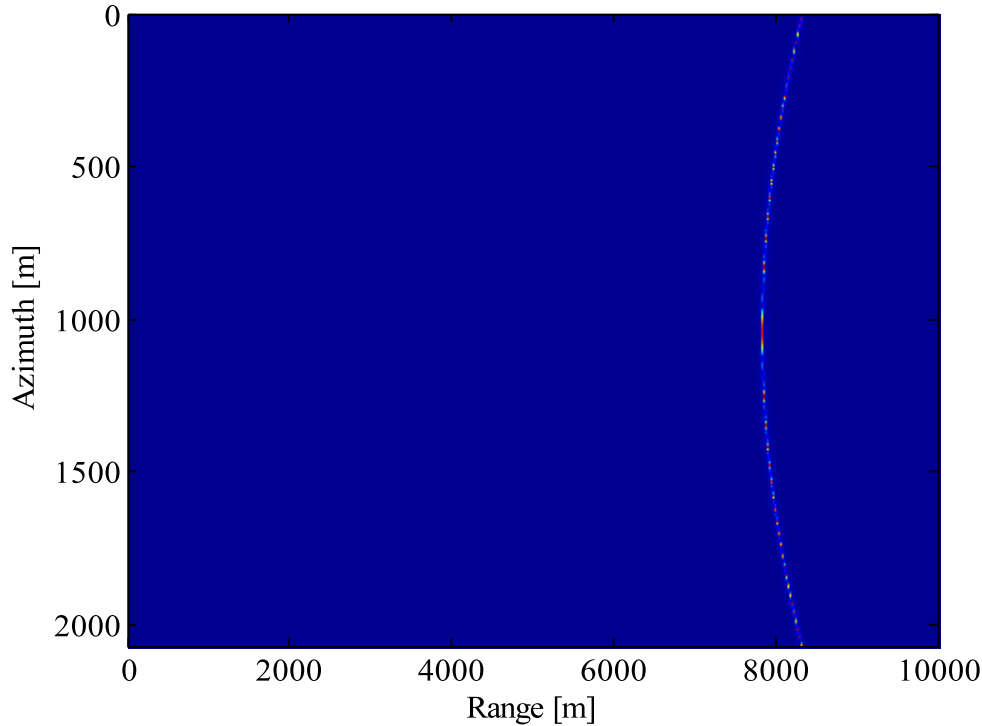
Figure 4.1: Received SAR data in two-dimensional signal memory.

signals to deal with), an efficient method to evaluate the discrete convolution named **overlap-add method (OA,OLA)** [19, 20] has been preferred.

The Overlap-add method

This method is an important DSP technique which is used to deal with segments of a long signal for easier processing. Overlap-add method is used by the FFT convolution. This filtering method is particularly used when computer memory is not sufficient to store a big signal entirely. The overlap-add method had a role in the following way in our work — all received compressed pulses, that together constitute the entire signal matrix, are filtered individually by the FIR filter (the matched filter) created, and all the filtered signals are then stored in a new matrix.

Let us suppose, the long signal is $x[n]$ and the FIR filter is $h[n]$. Then, the convolution between these two quantities is

$$y[n] = x[n] * h[n] \tag{4.2}$$
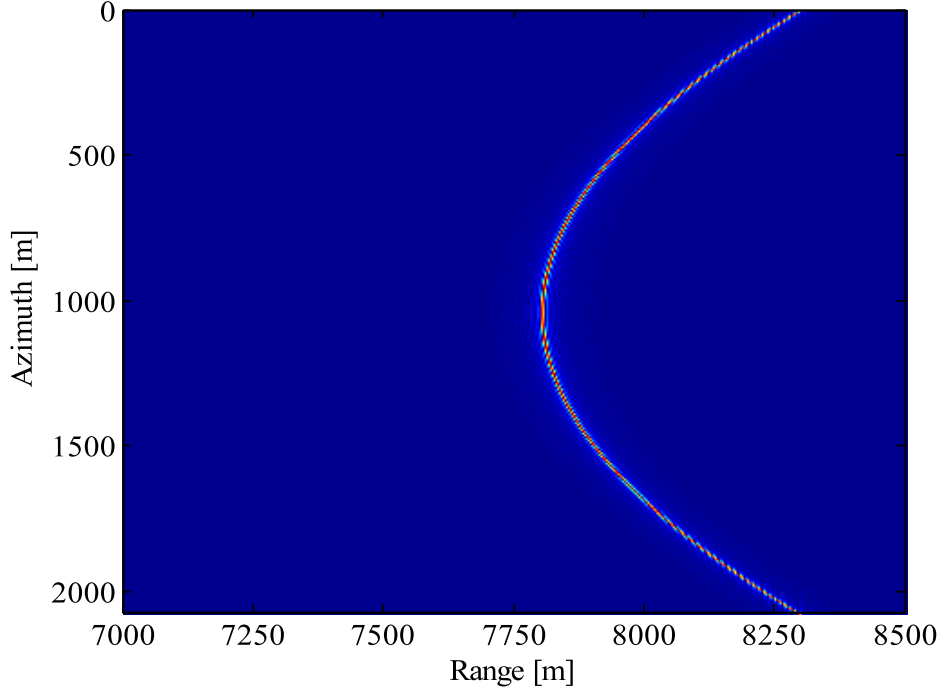
Figure 4.2: Received signal history curve shape in clear form. The strength of the signal received at the center of the aperture is maximum. Received signal strength gets reduced again as the aircraft moves away from the target.

If the signal is divided in k number of segments of arbitrary length L, then

$$x[n] = \sum_k x_k[n - kL] \tag{4.3}$$

Now $y[n]$ can be written as short convolution between $h[n]$ and each segment of the signal,

$$y[n] = \left(\sum_k x_k[n - kL] \right) * h[n]$$

$$= \sum_k \left(x_k[n - kL] * h[n] \right) \tag{4.4}$$

From (4.4), it is very clear that each segment of the signal is being convolved with the filter. This is the significance of the overlap-add method, reducing the load on the processor while processing a big signal.

4.2.2 Data Processing

The goal of any image formation algorithm is to gather information from the target by transmit and receive signals and then forming the image of that very point target by processing the signal data.

In GBP, a SAR image is directly produced from the radar echo data. There is no intermediate step between data acquisition and final image formation in this method. A stationary target, situated at some position on the ground, is placed at point (x, ρ) in the SAR image by the backprojection process in GBP, and this process in interpreted by the integral

$$h(x, \rho) = \int_{-\frac{L}{2}}^{\frac{L}{2}} g(x', r) \, dx' \qquad (4.5)$$

where, $h(x, \rho)$ is the backprojected signal, L is the aperture length, x' is the platform positions in the flight track and, $g(x', r)$ is the range compressed data of the stationary point target. For straight flight track, the range r to the point (x, ρ) in the image plane is represented by the hyperbolic function as

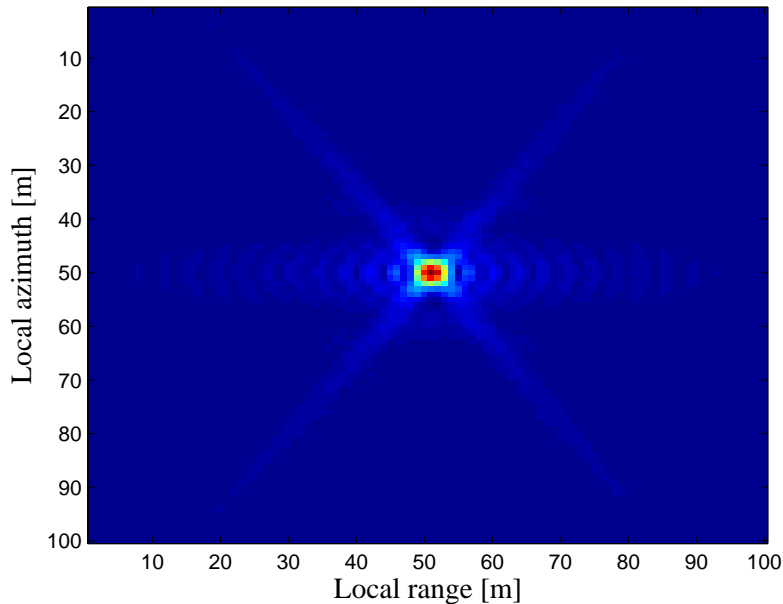$$r = \sqrt{(x' - x)^2 + \rho^2} \qquad (4.6)$$

Figure 4.3: SAR image of the point target obtained in GBP.

An area of 100×100 pixels was defined first in the implementation, and the range distances for signal transmission-reception were measured for every aperture position. The distance between the target and aperture points differs from point to point. These distances gave us the signal traveling time with which we could form an index that finally modified the signal matrix and formed the image matrix. Scaling the image data to the full range of colormap by appropriate command displays the image. Each element of the image matrix represents a rectangular area in the image. We see the SAR image of the point target in Figure 4.3.

Thereafter, the SAR image spectrum corresponding to this point target was produced by simple Matlab commands applied on the same image data. Figure 4.4 shows the 2-dimensional Fourier transform of the SAR image formed with GBP.
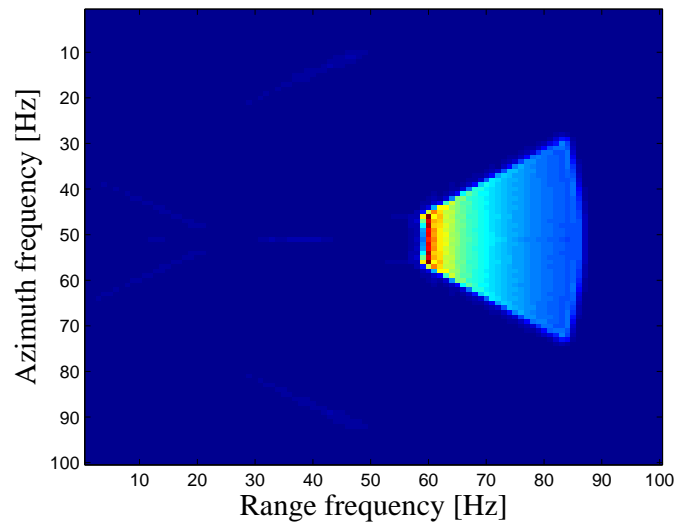
Figure 4.4: SAR image obtained in GBP in 2D frequency domain.

4.3   Image Quality and Processing Time

The SAR image spectrum shown in Figure 4.4 possesses some undesirable frequency components. These are actually such points where the approximation of the neighboring points has not been done accurately. To improve the image quality, these noises (white patches in the image) have to be removed. Upsampling the received signal data and use of proper interpolation methods could erase the undesirable frequency components from the SAR image spectrum to a great extent and produced better images. We have applied three interpolation methods (Linear interpolation, Nearest-neighbor and Sinc interpolation) in our code and tested the improvement. These methods have been discussed in detail in Section

3.4. Application of linear interpolation brought big difference in the SAR image as seen in Figure 4.5.

Figure 4.5: Spectrum of SAR image obtained in GBP after noise elimination by *Linear interpolation* method.

The images we got by nearest-neighbor and Sinc interpolation method do not differ much from the one obtained by linear interpolation. Normally, it is difficult to notice any difference in the SAR image spectra without graphical measurements. We see the images in Figure 4.6 and 4.7.

Figure 4.6: Spectrum of SAR image obtained in GBP after noise elimination by *Nearest-neighbor* method.
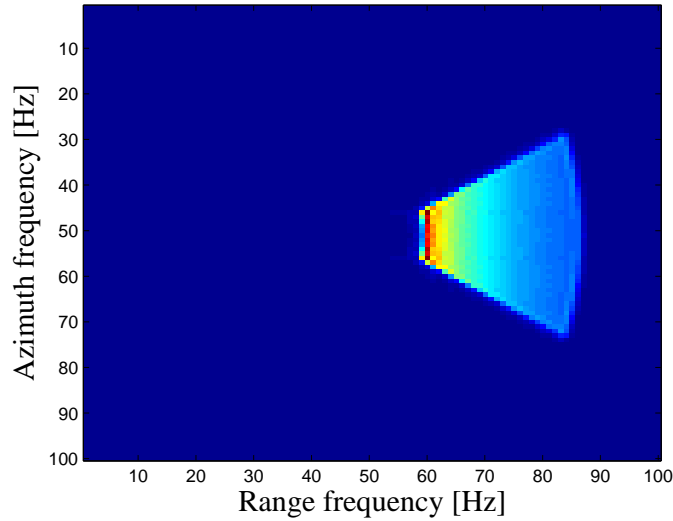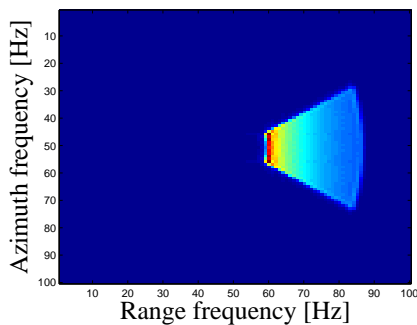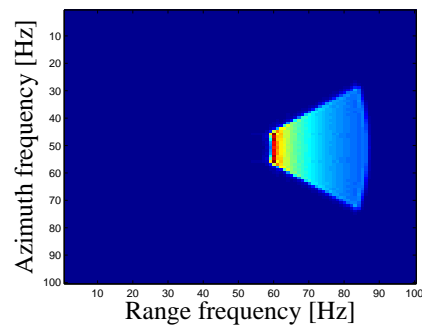
Figure 4.7: Spectrum of SAR image obtained in GBP after noise elimination by *Sinc interpolation* method.

The time elapsed to produce the images in the three interpolation methods have

been calculated using stopwatch timer in Matlab. We saw that, the shortest time
elapsed to form the image was in nearest-neighbor method and, the Sinc inter-
polation method required the maximum time. Table 4.2 shows the results.

Table 4.2: Processing times in interpolation methods.

Method	Time (t)
Linear interpolation	0.0096
Nearest-neighbor interpolation	0.0059
Sinc interpolation	0.0550

4.4   Motion Compensation in GBP

In the implementation of the GBP algorithm, we have considered an ideal state
(non-benign) of the flight track so far i.e., we have assumed that the flight track
is straight. But in practical case, such ideal straight track is impossible. The
aircraft will deviate from its straight track due to wind or other practical issues.
The direction of motion of the aircraft could fluctuate both horizontally and ver-
tically. We have considered a deviation of 15 m and 100 m in the horizontal
and vertical directions respectively. The change in position of the radar platform
was chosen to be random in this implementation. For frequent change in aircraft
position, the received signals were found to be distributed still holding the curved
shape. The signal history, encountering motion compensation, is shown in Figure
4.8.

The term 'motion compensation' is taken into account when the SAR platform
moves in a non-linear path. When projecting the signal data i.e. collecting the
echo signal, the distances between SAR and target and, corresponding time de-
lays were calculated for every randomly distributed SAR positions. Therefore,
when backprojecting the data to the image space, it has been done with ref-
erence to the corresponding very positions where from the echo data had been
collected. Thus, the possibility of getting spurious SAR image is avoided. If the
data were received at randomly fluctuating SAR positions but, backprojection
was done with respect to linear ideal positions, the correct SAR image would not
be produced. Consideration of the same platform positions for the projection
and backprojection of data is providing the correct image. This is like resisting
the damage in image quality due to fluctuating SAR positions, by backprjecting
the data from the same positions.
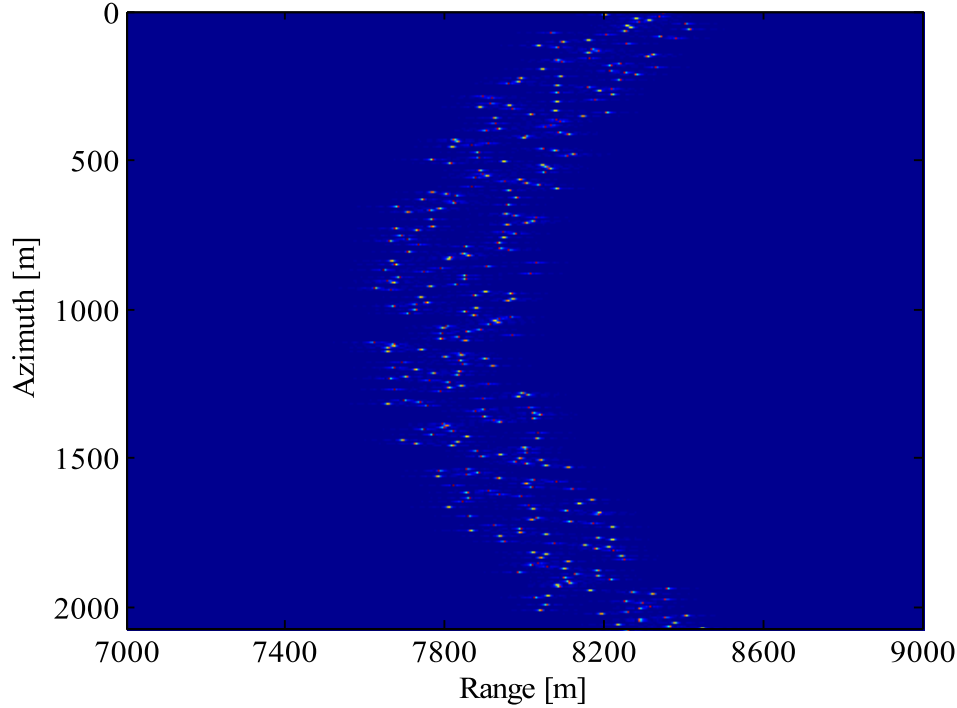
Figure 4.8: Received signal history with motion compensation encountered.

$$R_{Pr} = \sqrt{(X_{pf} - X_{tg})^2 + (Y'_{pf} - Y_{tg})^2 + (Z'_{pf} - Z_{tg})^2} \qquad (4.7)$$

Equation (4.7) shows the projection ranges while collecting the reflected signals, where, $(X_{pf}, Y'_{pf}, Z'_{pf})$ represents the SAR positions and, (X_{tg}, Y_{tg}, Z_{tg}) represents the target position. The 'primes' denote the random platform positions in the horizontal (Y) and vertical (Z) directions. Equation (4.8) shows the ranges when backprojecting the signal data over the image space $x_{im} \times y_{im}$. d determines the starting position of data placement over the image space.

$$R_{BP} = \sqrt{[X_{pf} - (X_{tg} - d + x_{im})]^2 + [Y'_{pf} - (Y_{tg} - d + y_{im})]^2 + [Z'_{pf} - Z_{tg}]^2}$$
$$(4.8)$$

If the backprojection was done with reference to linear flight track while the data had been collected for fluctuating track, it would result in bad quality imagery. In both (4.7) and (4.8), the same random SAR positions have been considered. Hence we see that, in GBP, the same quality image is obtained for fluctuating flight track as obtained for straight track, and the motion compensation is

done automatically. Figure 4.9 and 4.10 show the SAR image and its spectrum respectively, the image quality of which are the same as in Figure 4.3 and 4.5.
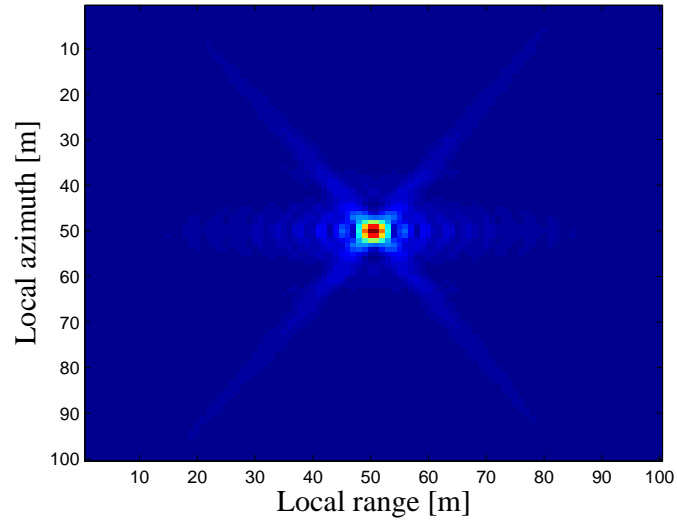

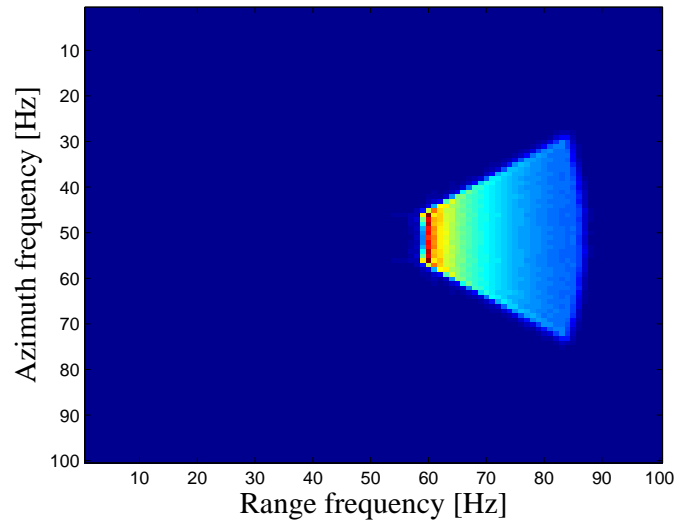Figure 4.9: SAR point target image after motion compensation.

Figure 4.10: Spectrum of the SAR point target image after motion compensation.

Chapter 5

Local Backprojection

5.1 Introduction

The Local Backprojection (LBP) algorithm is the main topic of this thesis. GBP could be considered as a basic algorithm for the implementation of the others following it and for illustration of their different comparable features. The computational load in LBP is lower than in GBP. Calculation of the computational load for LBP and, a comparison of its result to that for GBP has been shown in Section 5.2. The signal data acquisition is performed in the same way as in GBP, but the processing of the data is done in a different style. LBP is a two-stage algorithm. In GBP, the image could be formed directly from the data; whereas in LBP, *beamforming* is done as an intermediate step from which the final point target image is produced. The essence of the LBP algorithm lies in the fact that – the full aperture is divided into subapertures, the entire image space is divided into several subimages, and the beams of one subaperture have influence over all subimages. The signal processing is performed *locally* for each subimage individually and, thus part of the full image is formed. Later, all the subimages are combined together to produce the complete point target image.

5.2 Computational Load Calculation

For GBP

As we have seen in Chapter 4, for an $N \times N$ image and N_a number of total aperture positions, the computational load for GBP becomes,

$$N_{op} = N_a \times \left(N \times N \right) = N_a \times \left(N^2 \right). \tag{5.1}$$

For LBP

The computational load for LBP obtained according to this implementation is,

$$
\begin{aligned}
N_{op} &= N_{sa} \times \left(N_{si} \times \left(N_{a,sa} \times N_b + N \times N \right) \right) \\
&= N_{sa} \times N_{si} \times N_{a,sa} \times \left(N_b + \frac{N^2}{N_{a,sa}} \right) \\
&= N_a \times N_{si} \times \left(N_b + \frac{N^2}{N_{a,sa}} \right) \\
&\approx N_a \times \left(\frac{N^2}{N_{a,sa}} \right).
\end{aligned}
\tag{5.2}
$$

where,
N_{sa} – Number of subapertures,
N_{si} – Number of subimages,
$N_{a,sa}$ – Number of subaperture positions,
N_b – Number of beam samples,
N – Number of pixels in the azimuth or, range, and,
N_a – Total number of aperture positions ($N_a = N_{sa} \times N_{a,sa}$).

It is evident from (5.1) and (5.2) that, the computational load for LBP is $N_{a,sa}$ times lower than that for GBP.

5.3   Data Processing

The most eye-catching feature of LBP algorithm, that makes it distinct from GBP is that the whole image is segmented in parts (subimages) and the computation of the reflectivity of the surface points is done locally in every part separately, whereas the entire image space was considered in GBP. Also the azimuth flight track is divided in number of subapertures, with certain number of aperture points in it. The reflectivity of the surface points in the image space is computed within the subimage for each subaperture. The image space is defined along the azimuth and the slant range in the same length.

5.3.1   Beamforming

Beamforming is the pre-stage of final image formation in LBP. According to [2], the backprojected signal for GBP was defined as,

$$
h(x,\rho) = \int\limits_{-\infty}^{\infty} g\left(x', \sqrt{(x' - x)^2 + \rho^2} \right) \, dx'
\tag{5.3}
$$

The SAR image in GBP was found by solving the integral (5.3) for each image point in the whole image space. To find the SAR image in LBP, there are some differences in consideration in the aperture length and image area. The total aperture length is divided into number of subapertures each consisting of certain number of flight positions. The image area is also segmented in different number of subimages. In LPB, the backprojection integral is solved over approximately M subapertures each with length L_s over one subimage for one subaperture position at a time. Therefore, the LBP at some point (x, ρ) in the image space can be defined as

$$h(x, \rho) = \sum_{m=1}^{M} \int_{x_m - \frac{L_s}{2}}^{x_m + \frac{L_s}{2}} g\left(x', R_{cm} + \frac{\{(x' - x_m) - (x - x_c)\}(x_m - x_c) + (\rho - \rho_c)\rho_c}{R_{cm}}\right) dx' \tag{5.4}$$

where, x_m is the center-point of the m-th subaperture, (x_c, ρ_c) is the center co-ordinate of a subimage, and $R_{cm} = \sqrt{(x_c - x_m)^2 + \rho_c^2}$, as seen in Figure 5.1.

Beams are calculated at every subaperture center point x_m over each subimage. The beams are superposition of pulses in subapertures and these are calculated over the full length L_s of a subaperture i.e. from 0 to L_s, with respect to the center position of a subaperture. Rewriting (5.4) we get,

$$\begin{aligned} &h(x, \rho) \\ &= \sum \int g\left(x', R_{cm} + \frac{(x - x_c)(x_c - x_m) + (\rho - \rho_c)\rho_c}{R_{cm}} + \frac{x_m - x_c}{R_{cm}}(x' - x_m)\right) dx' \\ &= \sum \int g\left(x', R_{cm} + \{(x - x_c)\cos\alpha + (\rho - \rho_c)\sin\alpha\} + (x' - x_m)\cos\alpha\right) dx' \\ &= \sum \int g\left(x', R_{cm} + r + (x' - x_m)\cos\alpha\right) dx'. \end{aligned} \tag{5.5}$$

where, r is the local range history, α is the angle between the azimuth line and the formed beam. Equation (5.5) represents the summation of the subaperture integrals. The subaperture integral is called the subaperture beam. From (5.5), therefore we can write the subaperture beam

$$y(r, m) = \int_{x_m - \frac{L_s}{2}}^{x_m + \frac{L_s}{2}} g\left(x', R_{cm} + r + (x' - x_m)\cos\alpha\right) dx'. \tag{5.6}$$

One beam is formed for each subimage. Primarily, we have considered to form *four* subimages i.e., we divided the image space in four parts of equal area. Hence, we got four subaperture beams as shown in Figure 5.2.
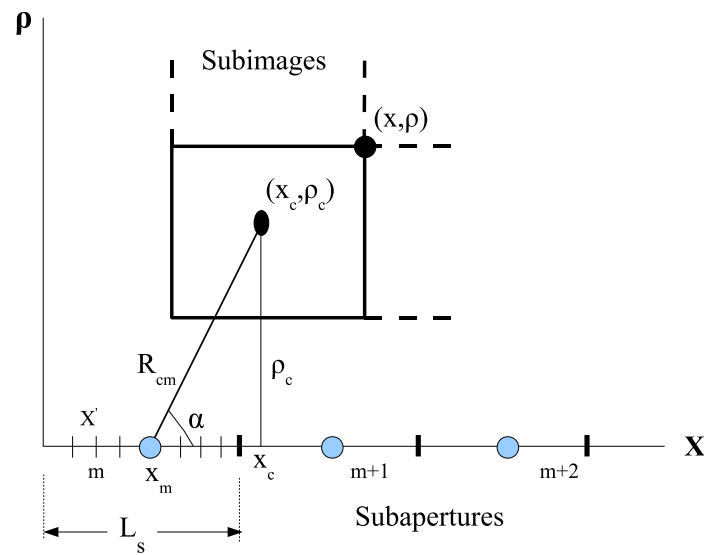
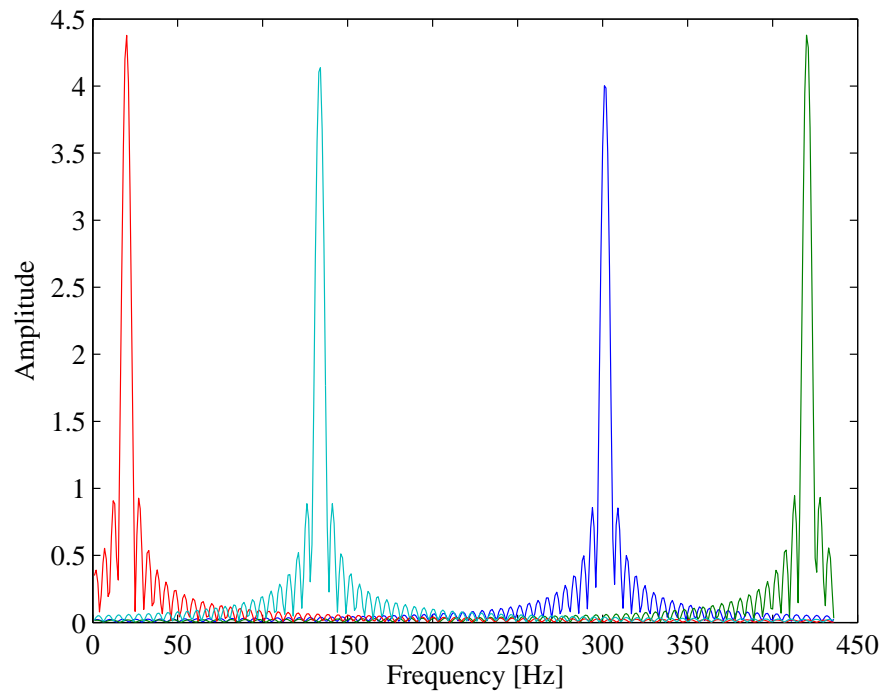Figure 5.1: Subaperture beamforming.

Figure 5.2: Subaperture beams.

5.3.2   Image Formation

The subaperture beams, formed in (5.6), are the prerequisite to form the subimages and eventually the full SAR image in LBP. Forming the beams from the signal data and taking the summation of the subaperture beams in order to produce the SAR image is the main theme of LBP. Now, if we write (5.5) in terms of subaperture beam got in (5.6), we get the LBP equation as

$$h(x, \rho) = \sum_{m=1}^{M} y\bigg((x - x_c)\cos\alpha + (\rho - \rho_c)\sin\alpha, m \bigg). \qquad (5.7)$$

Equation (5.7) is the final equation, the implementation of which gives us the subimages. The final SAR image is a combination of subimages. We created four subimages as mentioned earlier, and then we arranged them to form the complete SAR image of the point target. Figure 5.3 shows the SAR image of the point target after combining the subimages. Maximum information are placed at one corner of every subimage, and those are arranged in such order in a matrix that all the maximum information holding corners meet each other at the center of the image space. Thus, we got the full image. However, a wrong combination of subimages gives error in the full image, and an example of how an incorrect image could look like has been shown in Figure 5.4.
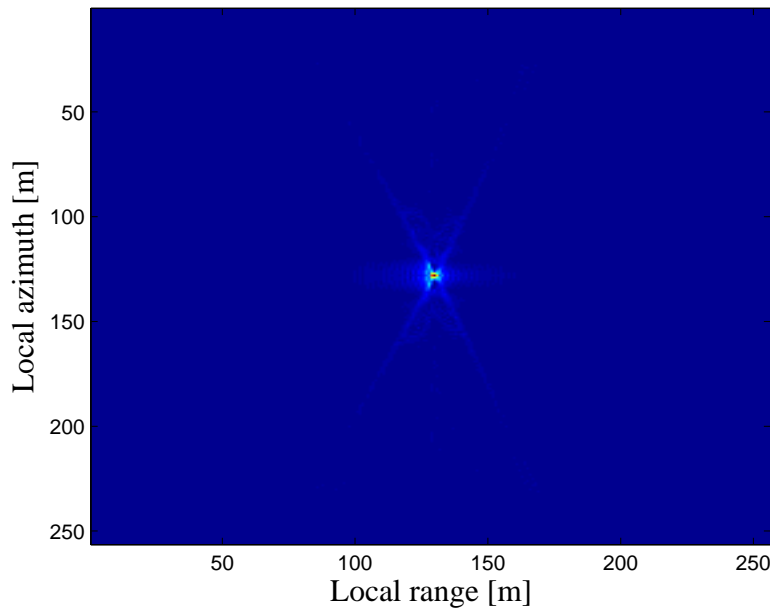

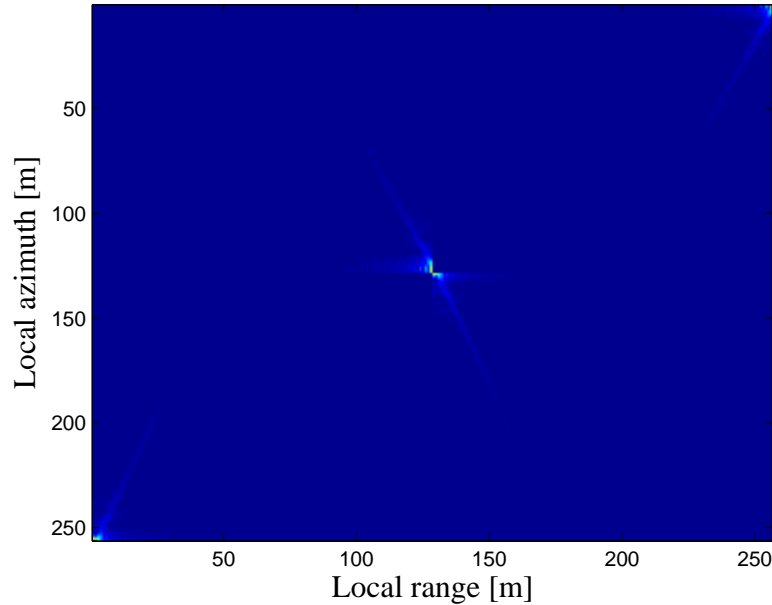Figure 5.3: SAR image of the point target obtained in LBP.

Figure 5.4: Incorrect image with wrong combination of subimages.

5.4   Image Quality Enhancement

In Figure 5.3, the left edge of the point target does not look very sharp and a tendency of flaring in that edge is noticed. This tendency is clearer in Figure 5.5 when upsampling of the signal data has been performed. Figure 5.3 and 5.5 are produced with four subimages. Segmenting the image space in more than four subimages (always in the order 2^{2n}; n=1, 2, 3,... within the image size) could erase the noise and we got nicer image. Later on, the image space was divided in 16, 64 and even in 256 subimages (i.e. one subimage for one pixel in case of 256), and significant improvement in image quality has been noticed. SAR point target images with increased subimage numbers are shown in Figure 5.6, 5.7 and 5.8. It is obvious from these images that images with degraded quality are comprised of less number of subimages. The more we increase the subimage number, the better quality images are obtained. The impact of amount of subimages over image quality has been discussed in Section 5.5. Correspondingly, a difference in the SAR images in 2D frequency domain (SAR image spectrum) is also noticed. Figure 5.9 shows the 2D Fourier transform of the SAR image for 4 subimages before upsampling. The impact of upsampling is clear in Figure 5.10(a) where the SAR image still consists of 4 subimages. This is a much nicer SAR image than obtained before. With the increment of subimages, the SAR image spectra also get a better look than the ones got so far which is observed in Figure 5.10(b, c, d) with 16, 64 and 256 subimages respectively.
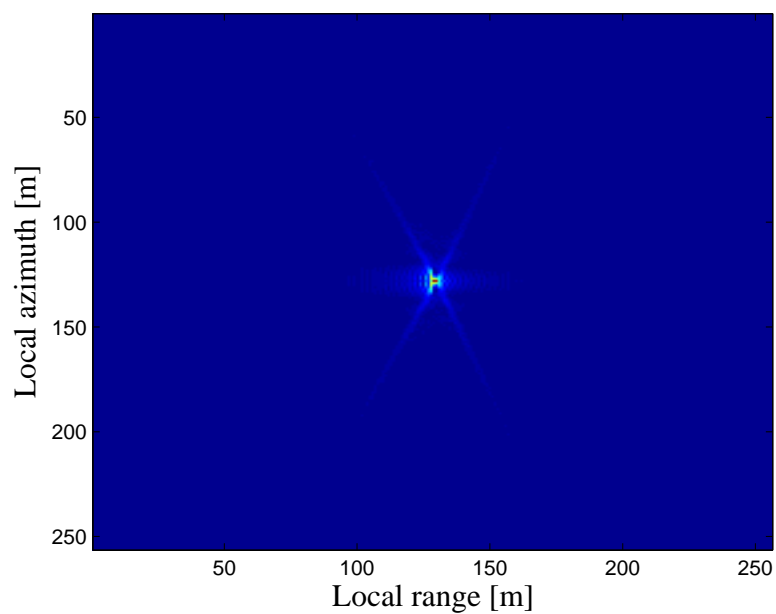
Figure 5.5: SAR image of the point target in LBP after upsampling.

Figure 5.6: SAR image in LBP formed with 16 subimages.
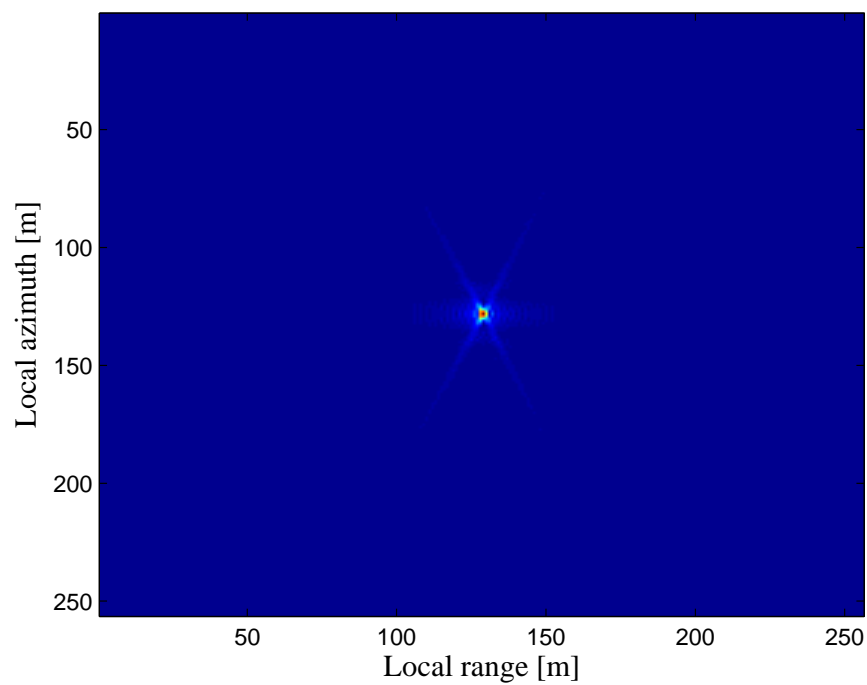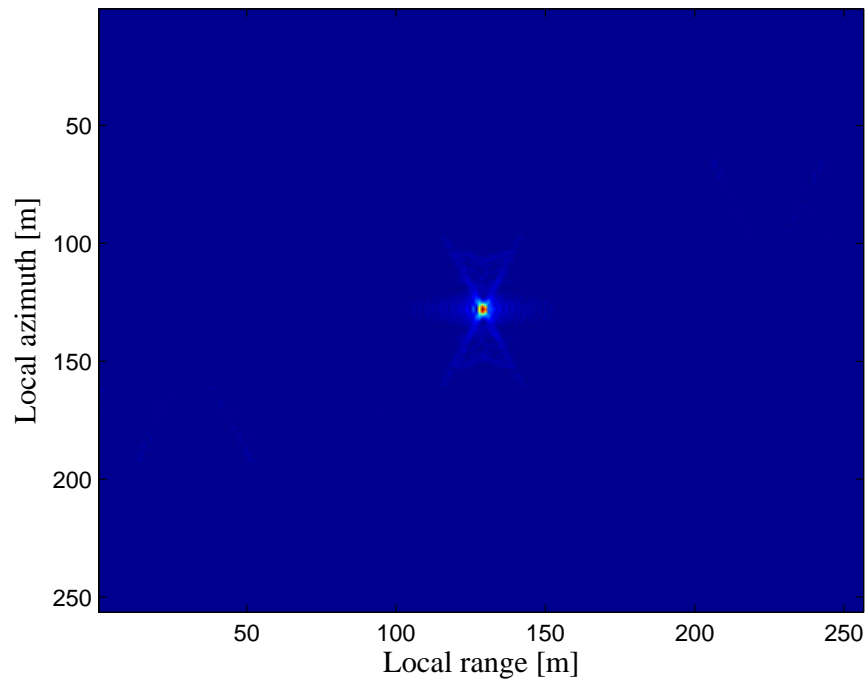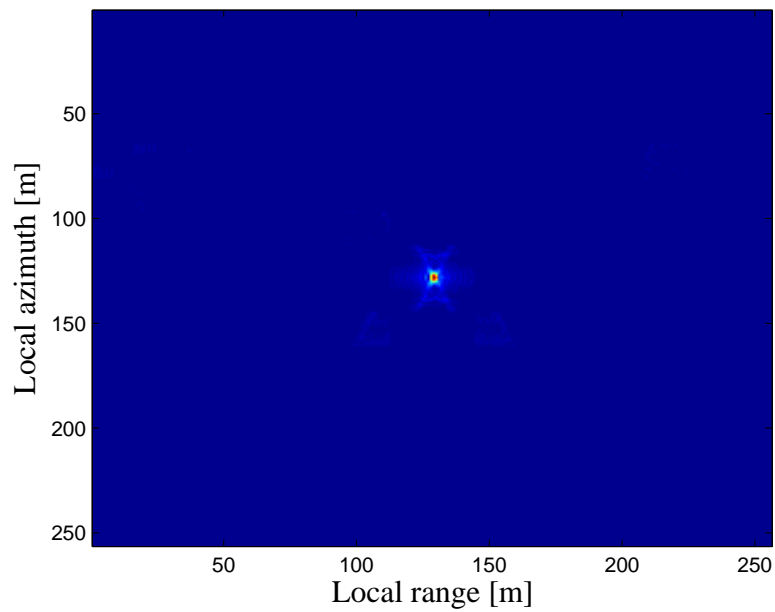
Figure 5.7: SAR image in LBP formed with 64 subimages.

Figure 5.8: SAR image in LBP formed with 256 subimages.

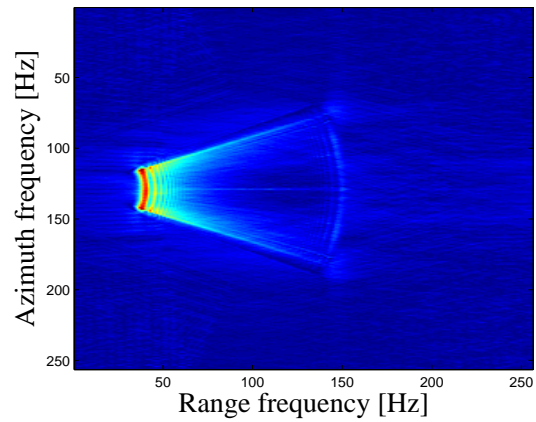Figure 5.9: SAR image spectrum obtained in LBP (with 4 subimages).

(a) With 4 subimages (after upsampling)

(b) With 16 subimages

(c) With 64 subimages

(d) With 256 subimages
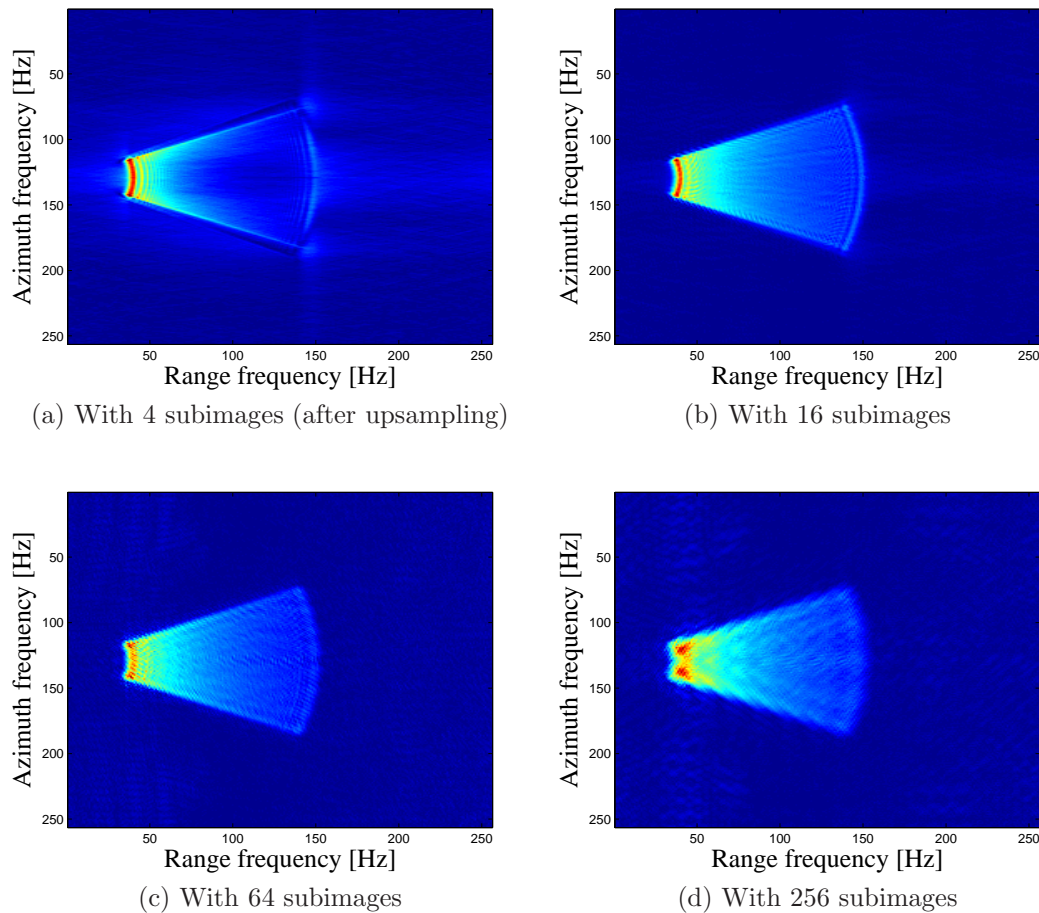
Figure 5.10: SAR image spectrums for different number of subimages.

5.5   Impact of Number of Subimages over Image Quality

In LBP, as we know, the complete aperture is split in subapertures and the image space is segmented in subimages. The reflectivity of every point on the surface within a subiamge with respect to each subaperture is mapped over the image space by backprojection. The more the subimage areas are smaller, the contribution of the subaperture points over the subimages was found stronger. The aperture blocks consist of 16 flight positions in our study. We have varied the subimage numbers within the 256×256 area. So, when subimage numbers are increased within that confined area, their own areas get smaller simultaneously. Thus, in the subimages, the distance of the diagonally formed beams from the corners of the subimages is short for small subimage size. That means the approximation of the nearest point from the beam during interpolation is more accurate for smaller subimages. This is illustrated in Figure 5.11. Therefore, an image with better resolution is obtained for smaller subimages by increasing the subimage number.

The point target is in far-field if the distance of it from the platform is compared to the wavelength of the signal ($R = 2D^2/\lambda$; R=distance, D=antenna dimension, λ=wavelength).
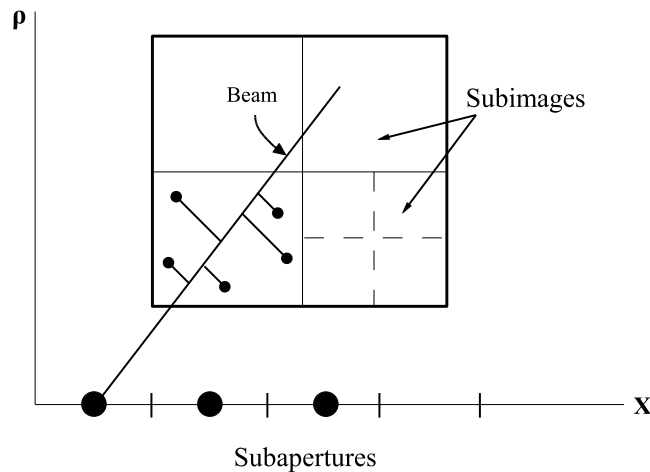
Figure 5.11: The effect of small subimage area.

5.6   Summary

In this chapter, we have implemented the LBP. Image formation in this algorithm reduces the computational load on the SAR processor by approximations of similar points along a line (beam) and then backprojecting locally in the subimage, rather than calculating line integrals for every pixel in a subimage. It is a unique feature that it divides the full image area for convenience in processing. The imagery, thus formed, are also of good quality since greater concentration is given upon a small sphere at a time. There is a contribution from every subaperture toward every pixel in a subimage and this is the integral along a straight line, which is the subaperture beam. The SAR images formed from the beams have been shown.

Chapter 6

Evaluation of The Local Backprojection Algorithm

6.1 Introduction

Evaluation of any system or algorithm depends on its performance to provide the result it is supposed to. Generally, the evaluation of an algorithm could be performed by measuring its ability to give a presumed result. Or, sometimes the evaluation could also be performed by attempting to test the algorithm with different data set that differs much from some standard data for the varying parameters. In the latter case, there may not be any presumed result always and just an investigative research is done.

In our research, here we will estimate the performance of the LBP algorithm. The estimation would be based on the quality of the SAR point target image and the SAR image in 2D frequency domain. The parameters that could be varied for the evaluation purpose are the integration angle, altitude and ground range of the platform, PRF etc. But some of these parameters are related to one another in a way that the variation in one parameter changes the other as well. A change in integration angle simultaneously changes the value of some other related parameters. The aperture length is dependent on the integration angle. The aperture length could also be varied by changing the altitude and ground range. However, the integration angle is found to be a single key parameter the variation of which is easy and, ultimately we make the same case as obtained by variation of two or more parameters.

6.2 Impact of Integration Angle over Images

The integration angle is the angle between the slant ranges from the two extreme aperture points meeting at the target. In this study, the integration angle was

chosen to be 45°. All the images produced in GBP (Chapter 4) and LBP (Chapter 5) were for 45°. However, later on, the effect of the variation of the integration angle over the images has been investigated. We have tested it for 5, 15, 25, 35 and 45 degrees.
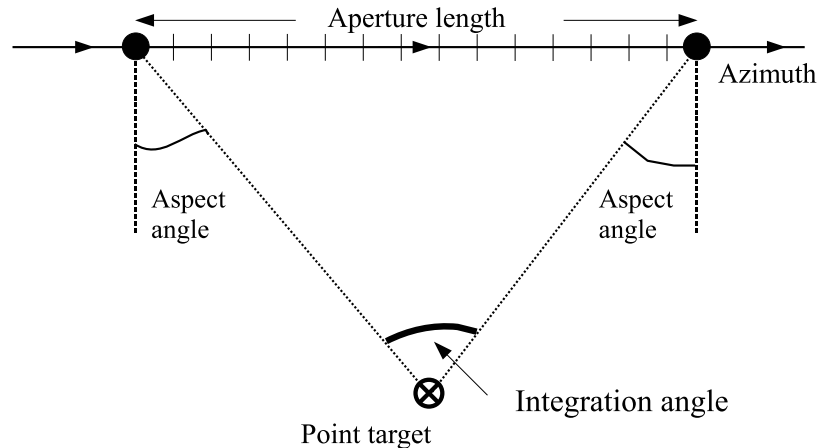
Figure 6.1: Integration angle.

6.2.1   Results for different values of Integration angle

The aperture length is directly proportional to the integration angle. For small angles, the aperture length gets shorter. Consequently, the signal history curve gets almost straight because the extreme SAR positions on the azimuth for small angle are not so distant from each other. This yields almost equal strength in the received signals. For bigger integration angles, SAR positions on the extreme edges of the aperture length get much distant. As we see from Figure 6.1, the aspect angle also gets bigger for bigger integration angles. So, the slant ranges to the point target for the extreme positions on aperture are also longer which makes the received signal strength weaker for these points. This phenomenon is the same for global backprojection also.

Now, the image results for different angles are shown below. All the tests results, to visualize the influence of different integration angles, have been shown for 4 subimages. The same images for different angles are shown together to make the difference prominent.

Signal history curve

In Figure 6.2, we see the signal history (collection of received signal) curves for different angles. All the figures shown here are zoomed in to the same degree in the X-axis to better understand the difference. The Y-axis length is determined according to the aperture position numbers. The X-axis represents the time-delay between transmit and receive signals.

For integration angle of 5°, the curve looks still (almost) straight even after zooming it in to a bit higher degree than for other angles. The reason is discussed earlier in Section 6.2.1. The increase in curvature of the curves is seen in Figure 6.2(b, c, d, e) for bigger angles.

SAR imagery of point target

Sophisticated processing of the collection of received signals gives the SAR image of the point target. For different integration angles, the shape of the point target changes also, and this is an effect of the signal history obviously. The resolution of the point target image depends on the amount of reflected signals and therefore, on the number of signal collecting points on the azimuth. For small number of such points, the imagery looks not very authentic. The information regarding exact position and nature of the target may not be gathered from such image. For very small integration angle, the edge of the point image may touch the defined image boundary and it would be treated as a spurious detection result. Gradually, when the angle and thus the aperture length have been increased, the point image looked nicer and more precise. That is what we see in Figure 6.3 for different angles.

For angle of 5°, the aperture length is very short and hence the number of subapertures is small. Therefore, the number of beam formation is less, that is not sufficient for good approximation of nearby pixel points in the image. As a result, we got a vertically stretched image due to poor resolution. For 15°, still the presumed shape of the target is not achieved but, the improvement in resolution is observed. As the angle was increased more, the number of subapertures and thus the number of beam formation increased. Finally, for angle of 45°, we got satisfactory resolution of the image.

SAR image spectrum

The effect of integration angle is very clear in the 2D Fourier transform of SAR images. No extra effort need to be given to notice the impact on these images. Figure 6.4 shows the SAR image spectra for different angles.

(a) For 5°

(b) For 15°

(c) For 25°

(d) For 35°

(e) For 45°
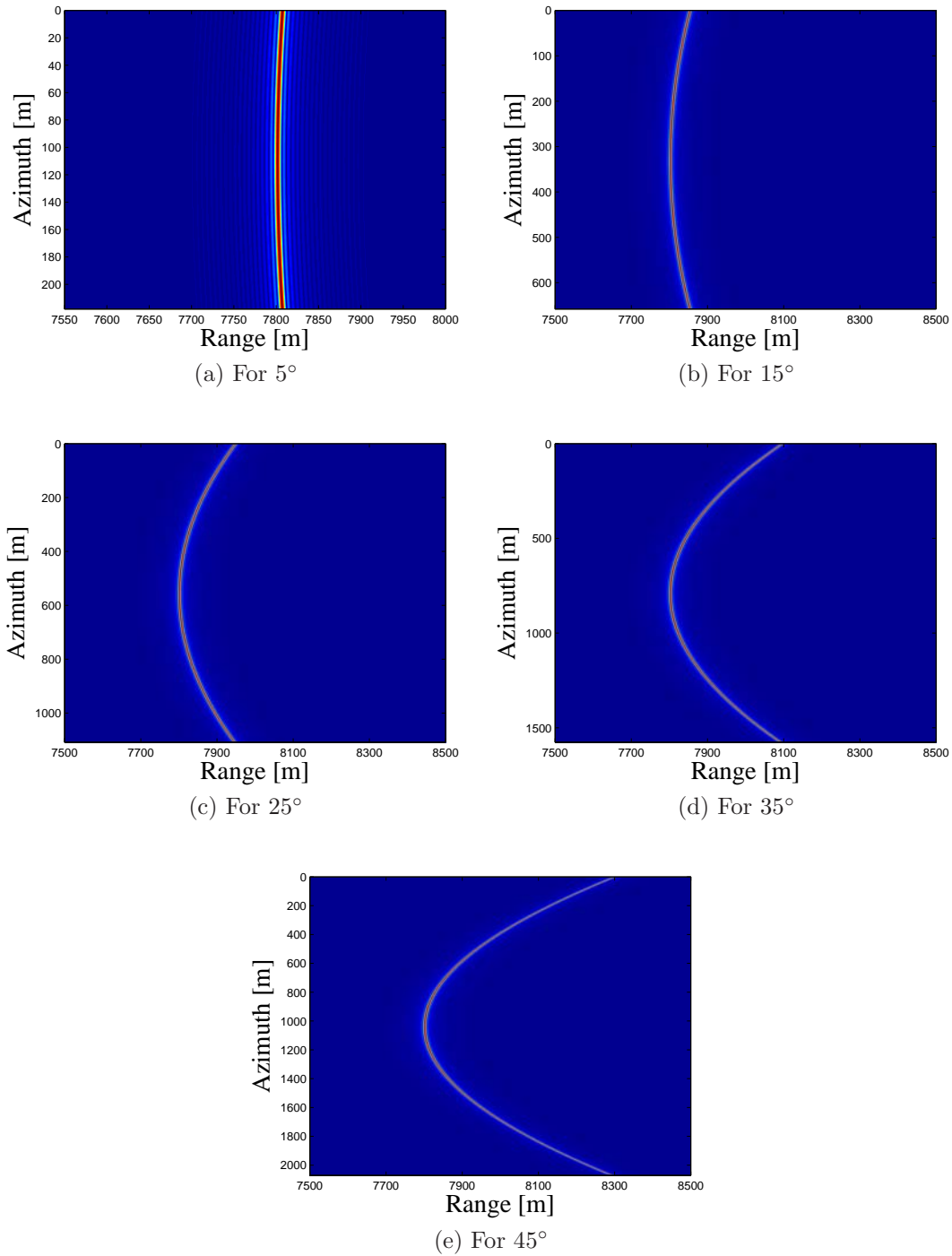
Figure 6.2: Signal history curves for different angles.

(a) For 5°

(b) For 15°

(c) For 25°

(d) For 35°

(e) For 45°
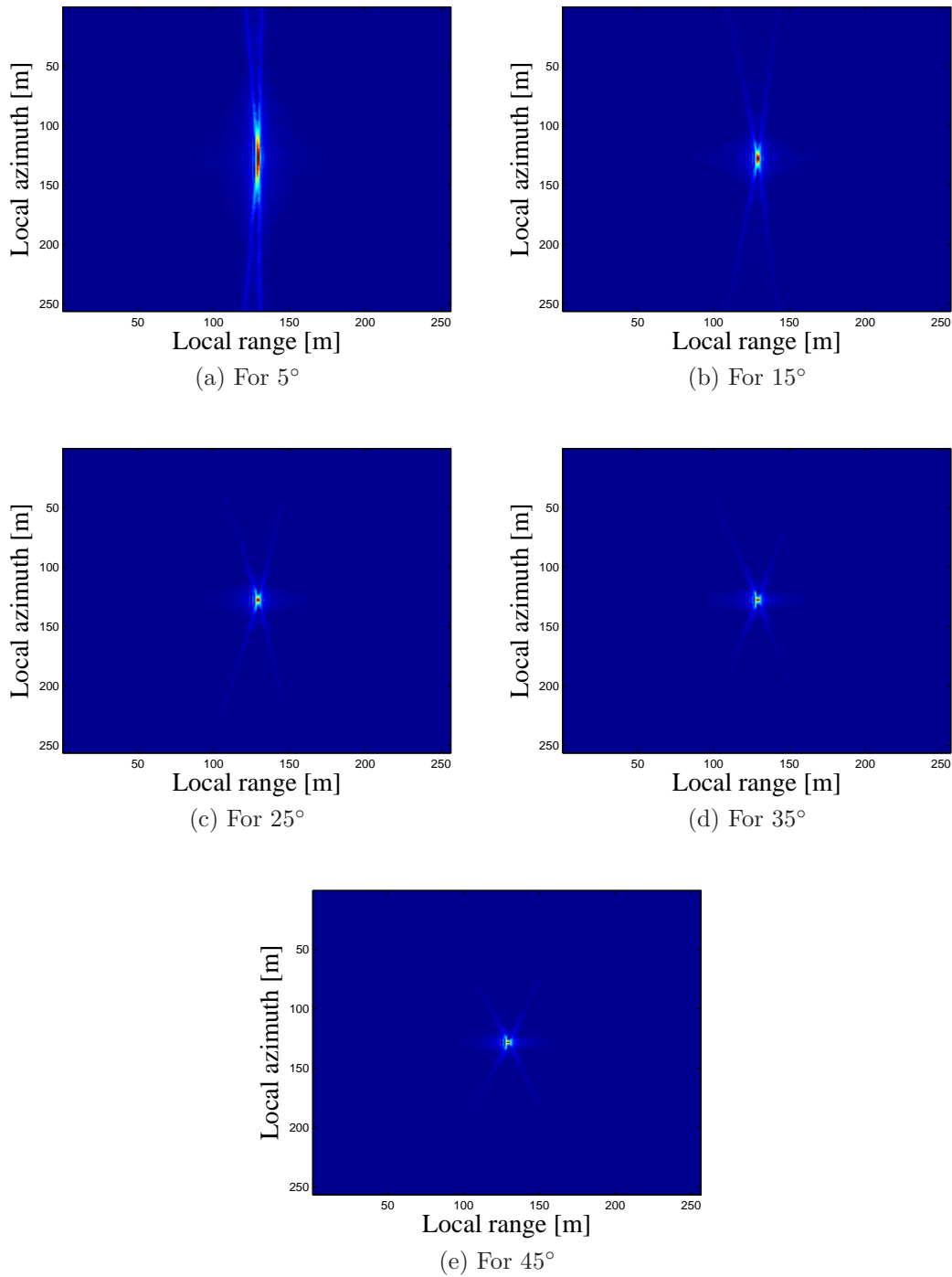
Figure 6.3: SAR image of the point target for different angles.

(a) For 5°

(b) For 15°

(c) For 25°

(d) For 35°

(e) For 45°

Figure 6.4: SAR image spectrums for different angles.

Chapter 7

Conclusion

7.1 Summary

Earlier in Chapter 2, the contrasting features of frequency and time-domain algorithms for radar imaging have been discussed once. We saw their advantages and some drawbacks in different aspects like, their performance in non-linear flight path, image processing speed, image quality etc. Global backprojection is the base of time-domain algorithms. In Chapter 4, GBP has been discussed in detail. The imaging has been shown for a stationary poin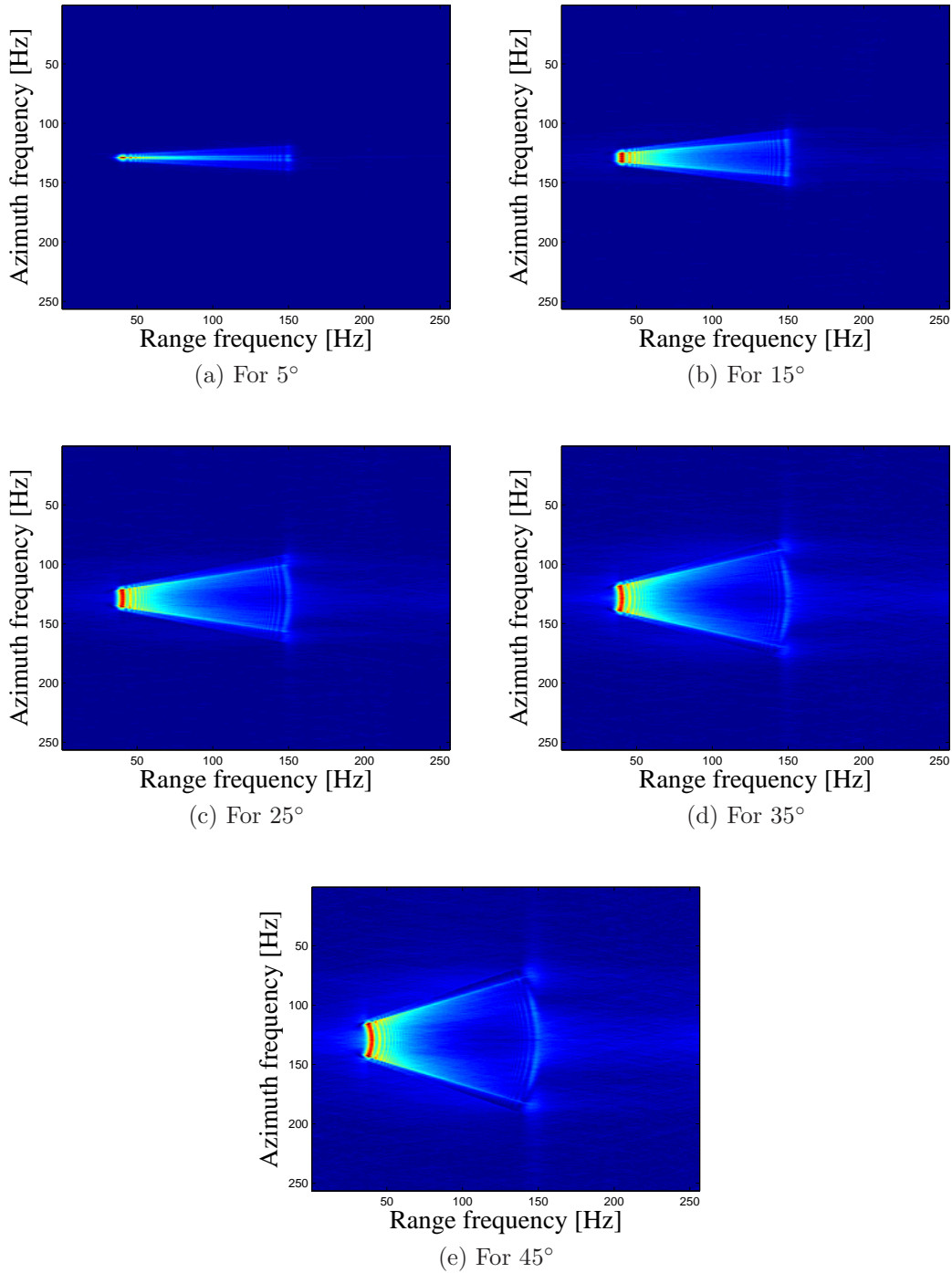t target. Information (signal) have been gathered from the target on ground first, and then processing that signal the image of the target produced. The same job has been done in the case of local backprojection also (Chapter 5). Same data set has been used for both methods. Since, the main topic of this thesis is the Local backprojection algorithm, an effort has been given also to evaluate the performance of it in Chapter 6.

The objective of this work was to study a still less popular SAR imaging algorithm (LBP). The dimension of the work was confined in just forming a point image and its SAR image. The goal of this thesis has been achieved. However, there are ample scope to work more with this algorithm.

7.2 Feasible Future Work

1. The point image for 4 subimages, in first place, was not so good in quality. A tendency to flare at the upper and lower left-corner has been noticed even after upsampling the data. This was removed to a good degree by increasing the subimage number. However, even if the best point target obtained here (for 256 subimages) is zoomed in, such flare is still noticed a little bit. This could be improved more to get a symmetric look on each edge of the image.

2. Both in GBP and LBP, upsampling of data and some interpolation methods have been applied for the enhancement of the image quality. However, no quantitative measurements have been done to estimate the difference.

3. An analytical comparison of this algorithm (LBP) with other time or, frequency-domain algorithms in the aspect of image quality by measuring spatial resolution, ISLR (Integrated SideLobe Ratio), PSLR (Peak Side-Lobe Ratio) etc. [21] would be an interesting topic.

4. The signal transmission from and reception on the radar platform is considered to be happened from the same geographical position [5] in this work. Later, a change could be brought by counting the Doppler effect as the platform moves on and it can be extended for spaceborne radar also.

5. In this thesis, only a stationary target has been considered. Local back-projection algorithm could be applied for detection and tracking of moving targets as well. This would be another very interesting extension of this work and a perfect sequel too.

Appendix A: List of Abbreviations

AIRSAR/TOPSAR   SAR system developed by NASA's Jet Propulsion Laboratory

CARABAS-II   Coherent All RAdio BAnd Sensing-II, (developed by FOI, Sweden)

CCRS-C/X-SAR   Canada Centre for Remote Sensing-C/X-band SAR

CHIRP   Compressed High Intensity Radar Pulse

CSA   Chirp Scaling Algorithm

DCS   Data Collection System

DSP   Digital Signal Processing

EM   Electro Magnetic

ERS-1   Earth Remote Sensing-1

FBP   Fast BackProjection

FFBP   Fast Factorized BackProjection

FFT   Fast Fourier Transform

FIR   Finite Impulse Response

FM   Frequency Modulation

FOPEN   FOliage PENetration

GBP   Global BackProjection

GMTI   Ground Moving Target Indicator

GPEN   Ground PENetration

IFSARE   InterFerometric Synthetic Aperture Radar for Elevation

ISLR   Integrated SideLobe Ratio

JERS-1   Japanese Earth Resources Satellite-1

LBP   Local BackProjection

LORA	LOw-frequency RAdar
MATLAB®	MATrix LABoratory, (a language of technical computing created by The MathWorks™)
OA/OLA	OverLap-Add method
P-3/SAR	Airborne system of Environmental Research Institute of Michigan
PFA	Polar Format Algorithm
PRF	Pulse Repetition Frequency
PSLR	Peak SideLobe Ratio
RADAR	RAdio Detection And Ranging
RADARSAT-1	Canadian SAR Satellite (1995)
RAR	Real Aperture Radar
RDA	Range Doppler Algorithm
RMA	Range Migration Algorithm
SAR	Synthetic Aperture Radar
SIR-C/X-SAR	Spaceborne Imaging Radar-C/X-band SAR
SNR	Signal-to-Noise Ratio
STAR-1 & 2	Canadian SAR systems operated by Intera Technologies of Calgary
TBP	Time Bandwidth Product
UWB	Ultra Wide Band
VHF	Very High Frequency
WB	Wide Band

Bibliography

[1] Seger O., Herberthson M., and Hellsten H., "Real Time SAR Processing of Low Frequency Ultra Wide Band Radar Data", *EUSAR'98– European Conference on Synthetic Aperture Radar*, pp. 489–492, May 1998.

[2] Pettersson M. I., "Detection of Moving Targets in Wideband SAR", *IEEE Transactions on Aerospace and Electronic Systems*, Vol. 40, No.3, July 2004, 780–796.

[3] Canada Centre for Remote Sensing, *http://ccrs.nrcan.gc.ca/resource/tutor/ fundam/chapter1/01_e.php*, Last visited: January 2008.

[4] U.S. Centennial of Flight Commission, *http://www.centennialofflight.gov/es say/Evolution_of_Technology/radar/Tech39.htm.* Last visited: February 2008.

[5] Barber, B. C., "Theory of digital imaging from orbital synthetic-aperture radar", *International Journal of Remote Sensing*, 6 (1985), 1009–1057.

[6] Ronald J. B., William C., Elizabeth V., and McCandless W. J., "Synthetic Aperture Radar imaging systems", *IEEE AES Systems Magazine*, November 1995, 15–23.

[7] Happ L., Kappra K. A., Ressler M. A., Sichina J. P., Sturgess K., and Le F., "Low-Frequency Ultra-Wideband Synthetic Aperture Radar – 1995 BOOM-SAR Tests", *IEEE 1996 National Radar Conference, Ann Arbor, Michigan*, May 1996, 54–59.

[8] European Space Agency, *http://earth.esa.int/applications/data_util/SAR DOCS/index.htm*, Last visited: September 2008.

[9] Ender J. H. G., "Space-time processing for multichannel synthetic aperture radar", *IEE Electronics & Communication Engineering Journal*, 1999, 29–38.

[10] Ender J. H. G., "Experimental results achieved with the airborne multichannel SAR system AER-II", In *Proceedings of the European Conference on Synthetic Aperture Radar*, (EUSAR'98), Friedrichshafen, 1998, 315–318.

[11] Coe D. J., and White R. G., "Experimental moving target detection results from a three-beam airborne SAR", *AEÜ International Journal of Electronic Communication*, 50, 2 (1996), 157–164.

[12] Raney R. K., Runge H., Bamler R., Cumming I. G., and Wong F. H., "Precision SAR processing using chirp scaling", *IEEE Trans. on Geosci. and Remote Sensing*, Vol. 27, pp. 786–799, July 1994.

[13] Bennett J. R. and Cumming I. G., "A digital processor for the production of Seasat SAR imagery", *In Proceeding of the International Conference on Seasat-SAR Processor*, Dec. 1979.

[14] Cafforio C., Prati C., and Rocca F., "SAR data focusing using seismic migration and techniques", *IEEE Transactions on Aerospace and Electronic Systems*, Vol. 27, pp. 194–207, Mar. 1991.

[15] Andersson L. E., "On determination of a function from spherical averages", *SIAM Journal on Mathematical Analysis*, Vol.19, No.1, pp. 214–341, Jan. 1988.

[16] Yegulalp A. F., "Fast Backprojection Algorithm for Synthetic Aperture Radar", *IEEE Radar Conference*, pp. 60–65, April 1999.

[17] Ulander L. M. H., Hellsten H., and Stenström G., "Synthetic-Aperture Radar processing using Fast Factorized Back-Projection", *IEEE Transactions on Aerospace and Electronic Systems*, Vol. 39, No. 3, JULY 2003, 760–776.

[18] Cumming I. G., and Wong F. H., "Digital Processing of Synthetic Aperture Radar Data : Algorithms and Implementation", *Artech House Inc., Norwood, MA*, 2005.

[19] Steven W. S., "The Scientist and Engineer's Guide to Digital Signal Processing", *www.dspguide.com/ch18/1.htm*, Last visited: June 2008.

[20] Wikipedia, "Overlap-add method", *http://en.wikipedia.org/wiki/Overlap-add_method*, Last visited: June 2008.

[21] Viet T. V., Sjögren T. K., and Pettersson M. I., "A Comparison between Fast Factorized Backprojection and Frequency-domain Algorithms in UWB Low-frequency SAR", *IEEE International Geoscience and Remote Sensing Symposium, IGARSS*, 2008.